The Pennsylvania State University

The Graduate School

Department of Civil & Environmental Engineering

SEISMIC RESILIENCE OF HIGHWAY BRIDGES

A Thesis in

Civil Engineering

by

Ashok Venkittaraman

Submitted in Partial Fulfillment
of the Requirements
for the Degree of

Master of Science

May 2013

The thesis of Ashok Venkittaraman was reviewed and approved* by the following:

Swagata Banerjee Basu
Assistant Professor of Civil Engineering
Thesis Advisor

Andrew Scanlon
Professor of Civil Engineering

Gordon Warn
Assistant Professor of Civil Engineering

Peggy Johnson
Professor
Head of the Department of Civil & Environmental Engineering

*Signatures are on file in the Graduate School

ABSTRACT

Highway transportation network is one of the important civil infrastructure systems. Various components of this system, especially bridges, are highly vulnerable to extreme natural hazards such as earthquakes. Extreme events can cause severe damage to highway bridges and thus can result in disrupted functionality of highway transportation systems. Bridge damage not only causes direct economic losses due to post-event bridge repair and restoration, but also produces indirect losses arising from network downtime and traffic delay. Therefore, it is always desirable to minimize these negative consequences from extreme events and to maximize disaster resilience of highway transportation systems.

Seismic retrofitting of highway bridges is one of the most common approaches undertaken by state Departments of Transportation (state DOTs) and by bridge owners to enhance system performance during seismic events. In this relation, this study evaluates the effectiveness of different retrofit techniques to enhance seismic resilience of highway bridges. The study considers a reinforced concrete bridge in La Cienega-Venice Boulevard sector of the I-10 freeway in Los Angeles, California. The bridge was severely damaged during the 1994 Northridge earthquake due to shear failure of one of the bridge piers. Post-event reconnaissance indicated that the failure was initiated from inadequate lateral confinement of bridge piers due to which vertical load carrying capacity of the bridge reduced significantly resulting in crushing of core concrete and buckling of longitudinal re-bars of bridge piers during the seismic event. Seismic vulnerability of the

as-built bridge is estimated through finite element (FE) analysis of the bridge under a suite of time histories that represent seismic hazard at the bridge site. Appropriate loss and recovery models are used to calculate seismic resilience of the as-built bridge. Three retrofit strategies are applied to the bridge to observe the effectiveness of these strategies in enhancing bridge seismic resilience in case the bridge was retrofitted prior to the earthquake event. Seismic vulnerability of retrofitted bridge models are estimated through time history analyses of these models under the same set of ground motions used for the as-built bridge. Seismic resilience of a highway bridge can be represented as a combined measure of bridge seismic performance and its recovery after the occurrence of seismic events. For each method of seismic retrofit, seismic resilience of the bridge is calculated. Difference in resilience obtained before and after bridge retrofits and the respective costs incurred are evaluated. Comparison of these values indicates the relative effectiveness of different retrofit techniques in enhancing the seismic resilience of the bridge. Results show that one of the retrofit strategies is most effective in enhancing the seismic resilience of the bridge, whereas other two strategies are not effective at all. Cost benefit analysis is performed to calculate the benefit obtained from the most effective retrofit strategy over a period of 30-80 years after bridge retrofit. Hence, results obtained from this study help in educated decision-making for selecting efficient and cost-effective seismic design and/or retrofit strategies for highway bridges.

Keywords: Concrete bridges, fragility analysis, resilience, sensitivity study, cost analysis

TABLE OF CONTENTS

LIST OF FIGURES

LIST OF TABLES

ACKNOWLEDGEMENT

First and foremost, I would like to express my deepest thanks to my advisor, Dr. Swagata Banerjee Basu for her valuable guidance and advice. She led by example, by supporting, inspiring and assisting in every way possible. There have been numerous instances when she has altered her busy schedule to accommodate discussions regarding this research. Without her support, guidance and advice, this project would not have been possible. I would like to thank my thesis committee members Dr. Andrew Scanlon and Dr. Gordon Warn for their time, inputs and guidance. I would like to take this opportunity to thank my colleagues and other staff and the Head of the Department of Civil & Environmental Engineering, Dr. Peggy Johnson for granting me access to the some of the best facilities in a timely manner. I would like to thank Mr. Gautham Ganesh Prasad, former student who worked with Dr. Banerjee, for not only valuable guidance regarding my thesis but for motivation and for being a living example. I would like to thank the Mid-Atlantic Universities Transportation Center (MAUTC; Project No.PSU-2012-01) for providing partial financial support to conduct this research.

Last but not the least I would like to thank my family for their continuous encouragement and support throughout my graduate study.

Chapter 1

Introduction

A natural disaster is the consequence of an extreme natural hazard like earthquake, flood, hurricane, tornado, and landslide. It leads to economic, human and/or environmental losses to a society. The resulting loss depends on the resistance of the affected population to survive against the disastrous event, called its resilience. Disaster resilience of a civil infrastructure system is defined in literature as a function that indicates the capability of the system to sustain a level of functionality over a period of time decided by owners or the society.

Bridges constitute a significant part of highway transportation systems that serve as a key mode for ground transportation, and sometimes act as an important feeder system to other modes of transportation such as railroad systems, port facilities and air travel. Damage of highway bridges due to extreme events may cause severe disruption to the normal functionality of highway transportation systems, which may have further impact on the performance of other modes of transport. Bridge damage not only causes direct economic losses due to post-event bridge repair and restoration, but also produces indirect losses arising from network downtime, traffic delay and business interruptions.

Shirole and Holt (1991) documented that about 823 bridges failed over a period of 40 years since 1950 due to extreme events such as earthquakes, fire and vehicle overloading. Failure of a large number of highway bridges was observed in California

during 1971 San Fernando, 1989 Loma Prieta and 1994 Northridge earthquakes. These extreme natural events severely disrupted the normal functionality of regional highway transportation systems (Penzien *et al*. 2003) and caused sudden and undesired changes in technical, organizational, societal and economic conditions of communities served by these systems. Prevention is better than cure - this simple yet powerful adage becomes of profound importance when such a disaster condition is thought of. Along this line, 'recovery' and 'resilience' have become key points in dealing with extreme events, if not to prevent completely, but to minimize their negative consequences and to maximize disaster resilience of highway transportation systems. Seismic retrofitting of highway bridges is one of the most common approaches undertaken by state Departments of Transportation (state DOTs) and by bridge owners to enhance system performance during seismic events. Types of seismic retrofit strategies applied to a bridge depend on various factors including bridge attributes and configurations, accessibility and seismic demand. Common seismic retrofit techniques for bridges include lateral confinement of bridge piers using steel or composite jackets, installation of restrainers at abutments and expansion joints, seismic isolation through bearings and installation of bigger foundations (Caltrans 2011, WSDOT 2011, Wright *et al*. 2011). While all these bridge retrofit techniques may be effective in mitigating seismic risk of bridges, adequacy of their application and relative effectiveness greatly depend on demand from seismic hazard specific to a bridge, enhancement in seismic functionality of highway transportation systems, and benefit to cost ratio for bridge retrofitting. In this relation, calculation of resilience is identified as a meaningful way to express loss and recovery of system functionality immediately after a natural disaster (Chang and Nojima 2001, Bruneau *et al.*

2003, Chang and Chamberlin. 2004, Shinozuka *et al*. 2004, Rose and Liao. 2005, Amdal and Swigart. 2010, Cimellaro *et al.* 2010). Seismic resilience of a highway bridge can be represented as a combined measure of bridge seismic performance and its recovery after the occurrence of seismic events. Therefore, calculation of bridge resilience before and after the application of a retrofit strategy will not only indicate the effectiveness of this strategy in improving bridge seismic performance, but also exhibit its impact on system functionality during seismic hazard.

This study evaluates effectiveness of various retrofit techniques to enhance seismic resilience of highway bridges. A reinforced concrete bridge in La Cienega-Venice Boulevard sector of Santa Monica (I-10) freeway in Los Angeles in California is selected as a test-bed bridge. This freeway runs across 8 states from Florida to the Pacific. In 1993, this freeway was reported to be the world's busiest freeway carrying an average daily traffic (ADT) of 261,000, approximately (U.S Department of Transportation, 2002). During the 1994 Northridge earthquake, the bridge under consideration was severely damaged primarily due to shear failure of one of the bridge piers. Post-event reconnaissance indicated that the failure was initiated from inadequate lateral confinement of bridge piers due to which vertical load carrying capacity of the bridge reduced significantly resulting in crushing of core concrete and buckling of longitudinal re-bars of bridge piers during the seismic event. Seismic vulnerability of the as-built bridge prior to the seismic event is estimated through finite element (FE) analysis of the bridge under a suite of time histories that represent seismic hazard at the bridge site. Appropriate loss and recovery models are applied to calculate seismic resilience of the as-built bridge. To observe the effectiveness of various seismic retrofit techniques in

enhancing bridge seismic resilience, three retrofit strategies are considered assuming that the bridge was retrofitted prior to the earthquake event. Seismic vulnerability of three retrofitted bridges is estimated, and for each method of seismic retrofit, seismic resilience of retrofitted bridges is calculated. First order second moment (FOSM) reliability analysis is performed to evaluate sensitivity of bridge resilience on various parameters associated with bridge vulnerability analysis and resilience estimation modules. A tornado diagram is also developed to understand sensitivity of various parameters and to further support the observation from FOSM analysis. Cost-benefit study is performed for a range of 30-60 years of service life of the bridge after retrofitting.

Chapter 2

Seismic Resilience

Past studies have defined and calculated resilience of various lifeline systems such as acute care hospitals, water and power transmission systems and transportation systems (Chang and Nojima 2001, Bruneau *et al* 2003, Chang and Chamberlin 2004, Shinozuka *et al.* 2004, Rose and Liao 2005, Paton and Johnston 2006,Amdal and Swigart 2010, Cimellaro *et al* 2010, Arcidiacono and Cimellaro 2012, only to name a few). In some of these studies, resilience is quantified using the parameter functionality. For water delivery system in Memphis, Tennessee, Chang and Shinozuka (2004) introduced multi-dimensional concept of resilience that may address technical, organizational, social, and economic aspects of a community after a natural disaster. They identified the need for new methods to be developed for the estimation of monetary losses. It is imperative that resilience models relate anticipated losses to the community's seismic performance goals. This literature developed resilience measures through a case study on the water delivery system in Memphis, Tennessee. A previously developed loss estimation model was considered that provided the starting point for quantifying resilience. The authors analyzed two seismic retrofit strategies and found that one improves community resilience over the status quo. The exercise demonstrated that the resilience framework can be valuable for guiding disaster mitigation and preparedness efforts.

The framework proposed by Bruneau and Reinhorn (2007) to calculate seismic resilience for a critical facility like hospitals, attempted to quantify resilience of a hospital

system. Impact of time to recovery is considered as a parameter for functionality. The proposed framework made it possible to relate probability functions, fragilities, and resilience in a single integrated approach for hospital facilities. Cimerallo *et al*. (2010) evaluate the seismic resilience of a regional system of hospitals. This analysis is based on recovery period, recovery functions and fragility functions. The fragility functions represent that the maximum response of a structure exceeds a given performance threshold. The authors identified different paths to recovery which could be estimated by different recovery functions.

In comparison with other lifeline systems, resilience study for highway transportation network is rather scarce. A recent study by Frangopol and Bocchini (2011) proposed the use of resilience as an optimization criterion for seismic rehabilitation of highway bridges.

As mentioned in all of these previous studies, loss due to a natural event and post-event performance recovery are the two major components to quantify disaster resilience of civil infrastructure systems. For a single seismic event, resilience is expressed in Eq. (1) as (Cimerallo *et al*, 2010):

$$R = \int_{t_{0E}}^{t_{0E}+T_{LC}} \frac{Q(t)}{T_{LC}} dt \qquad (1)$$

where t_{0E} represents the time when the extreme event E occurs and T_{LC} is a controlled time set to evaluate resilience. $Q(t)$ represents system functionality which can be expressed as a dimensionless function of time t. The greater the area under the functionality curve, higher the system resilience.

The analytical expression of $Q(t)$ constitutes a loss function and a recovery function of system performance during the period of system interruption due to the extreme event (Cimellaro *et al*. 2010). The mathematical expression of functionality $Q(t)$ is given as

$$Q(t) = 1 - L(I, T_{RE}) * [H(t - t_{oe}) - H(t - (t_{oe} + T_{RE}))] * [f_{rec}(t, t_{oe}, T_{RE})] \quad (2)$$

where $L(I,T_{RE})$ is the loss function, f_{rec} is the recovery function, I represents intensity of the event, and T_{RE} is the recovery time from event E. $H()$ is the Heaviside Step function discontinuous function whose value is zero for negative argument and one for positive argument. Calculation of loss requires information on system vulnerability under natural disaster. Following subsections describes system vulnerability, loss and recovery functions for seismic events.

2.1. Vulnerability of a system or system component

For highway transportation systems, bridges are generally considered to be the most seismically vulnerable components. This study measured bridge vulnerability in the form of fragility curves. Fragility curves represent the probability of bridge failure in a damage state under certain ground motion intensity such as peak ground acceleration or PGA (Banerjee and Shinozuka 2007 and 2008a). The analytical form of the fragility curve is given as

$$F(PGA_j, c_k, \zeta_k) = \Phi\left[\frac{\ln(PGA_j / c_k)}{\zeta_k}\right] \quad (3)$$

where PGA_j represents PGA of a ground motion j and k represents different bridge damage states such as minor, moderate, major damage and complete collapse. The two parameters c_k and ζ_k are fragility parameter for a damage state k. These parameters can be estimated by maximizing the likelihood function L:

$$L = \prod F(PGA_j, c_k, \zeta_k)^{r_j} [1 - F(PGA_j, c_k, \zeta_k)]^{1-r_j} \quad (4)$$

Here r_j = 0 or 1 depending on whether or not the bridge sustains the damage state k under j^{th} ground motion.

Other intensity measures such as peak ground velocity (PGV), spectral acceleration (SA), spectral velocity (SV) and spectral intensity (SI) can also be used to represent seismic intensity. However, the use of any of the above intensity measures in development of seismic fragility curves provides no additional advantage over the use of PGA (Prasad and Banerjee 2013).

2.2. Loss function

The total losses resulted from an extreme event can be divided into two categories: Direct Losses and Indirect Losses. There have been various studies and different loss models to arrive at these values.

Mackie *et al*. (2009) discuss an improvised methodology for developing probabilistic estimates of repair costs and times that can be applied to evaluate the performance of existing bridges for future earthquakes or exploring new bridge design options. It uses the concept of performance groups that account for damage and repair of

individual bridge components. They adopt a disaggregation approach by splitting the system into individual components such as columns and these are denoted as performance groups. Finally, approximate Repair cost ratios and repair efforts are estimated from assembly of damage states from all groups.

Frangopol and Bocchini (2011) use a cost model as a function of time of rehabilitation (as it considers discount rate) and the damage recovery rate; they also use a reference for the rehabilitation cost for bridges as one fourth of its total cost. A bi-objective optimization is performed to maximize the resilience function over a given time and minimize this cost function. Various constraints for maximum cost, recovery rate and other parameters are applied.

Cimellaro *et al.* (2010) subcategorized the loss model further into economic and casualties losses for a system of hospitals. The study considers the value of the building to be affected by the discount rate, which is in turn affected by the depreciation rate. The direct structural losses are obtained component wise: structural and non-structural. The casualties' losses are calculated as a ratio of number of dead or injured to the total number of occupants.

For this study, the losses are computed in the following manner:

1. Direct Losses (L_D): These losses include the cost associated with post-event repair and rehabilitation of damaged structural components. They occur immediately after the disaster. For a bridge, direct economic loss resulted from an event *E* can be evaluated as (Zhou et al. 2010, Banerjee and Ganesh Prasad 2012)

$$C_{rE} = \sum_{k=1}^{n} P_E(DS = k) C r_k \quad (5)$$

where k represents the damage states of the bridge (such as minor, moderate, major damage and collapse states), P_E ($DS = k$) is the probability that the bridge can sustain a damage state k during the seismic event E. These values can be obtained from bridge fragility curves developed for various damage states. C represents the replacement cost which is evaluated by multiplying bridge deck area with the unit area replacement cost. r_k is the damage ratio corresponding to damage state k (HAZUS 1999). For the calculation of functionality, the present study uses a dimensionless cost term, L_D; that is the ratio of restoration cost with replacement cost. So the direct cost used in the present study is

$$L_D = \frac{C_{rE}}{C} = \sum_{k=1}^{n} P_E(DS = k) C r_k \quad (6)$$

2. Indirect Losses (L_I): These arise due to the disrupted functionality of the system due to the natural disaster. Indirect losses mainly consist of rental, income losses, relocation, business interruptions, traffic delay, losses in revenue from traffic to businesses served etc. These losses are time dependent. Indirect losses are the maximum at the day of the event and gradually reduce as bridge restoration takes place from past experiences and literature. The indirect losses due to increased travel time from bridge damage have been found to be 5-20 times greater than the direct losses from Dennemann (2009). To acknowledge these indirect losses, the total cost

of losses associated with each damage state is assumed to be 13 times larger than the estimated repair costs. This approach is adopted from Denneman(2009).

2.3. Recovery function

The recovery function (f_{rec}) describes a path following which post-event restoration of bridges is expected to take place. Development of an appropriate mathematical model for the recovery function involves extreme difficulty because of the dependence of post-event bridge recovery process on several factors including the availability of fund. According to actual bridge recovery processes after severe earthquakes in past, Zhou *et al*. (2010) proposed probabilistic distribution of post-event bridge recovery process. In this literature, time required to complete a bridge restoration is considered to be a random variable uniformly distributed between the maximum and the minimum required times to complete the restoration job. Cimerallo *et al*. (2010) took three recovery functions, linear, exponential or trigonometric; observe their effectiveness for system resilience.

Time required to complete a bridge restoration is not a unique quantity; it depends on the severity of bridge damage due to the extreme event. In HAZUS (Hazus®–MH MR5), bridge seismic recovery times at different damage states are modeled with normal distribution functions. Table 1 provides mean and standard deviations of restoration times for different bridge damage states.

Table 1: Mean and standard deviation of restoration times for different damage states (HAZUS)

Bridge damage state	Slight/Minor	Moderate	Extensive	Complete
Mean (Days)	0.6	2.5	75	230
SD (Days)	0.6	2.7	42	110

Chapter 3 Test-bed Bridge

The test-bed bridge considered in this study is a multi-span reinforced concrete bridge (Figure 1). The bridge connects the I-10 freeway and the La-Cienega Boulevard. Bridge superstructure is composed of 2.06 m deep and 1.58 m wide multi-cell hollow box girders. Cross-sectional and material properties of the bridge girder are obtained from Broderick and Elnashai (1994) and Lee and Elnashai (2002). The bridge is supported on six 1.219m diameter circular piers. Bent 5 is a multi-column bent with three identical piers supporting the bridge superstructure. Bents 6 to 8 each has single pier. Based on reinforcement, these piers have type 'H' and type 'M' cross sections (Figure 1). Bent 5 has type 'H' cross section and bents 6 to 8 have type 'M' cross section. Bent 9 has a rectangular wall section. All pier-girder joints connections are monolithic. Specific properties of these bents are further discussed later in this paper. The bridge has an in-span expansion joint just after Bent 6.

As the bridge is a part of freeway system, it is difficult to numerically simulate the accurate boundary condition of the bridge. Broderick and Elnashai (1994) developed four finite element models of the bridge by changing its boundary conditions. Effectiveness of these four models was judged by comparing the numerical response of the bridge with that recoded in real time during the Northridge earthquake. This comparison showed that fixed boundary on freeway side and hinged boundary (i.e., moment release) on the other side provided the closest match with recorder bridge response.

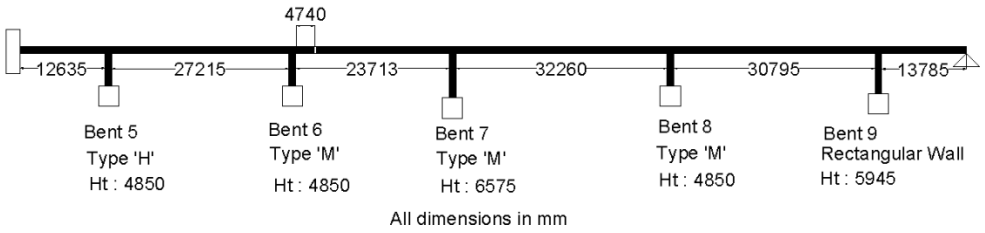

(a) Schematic diagram of the test-bed bridge

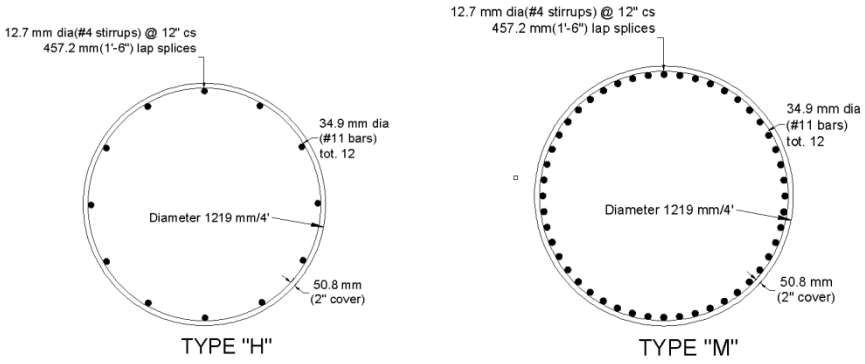

(b) Cross- Sections of the piers

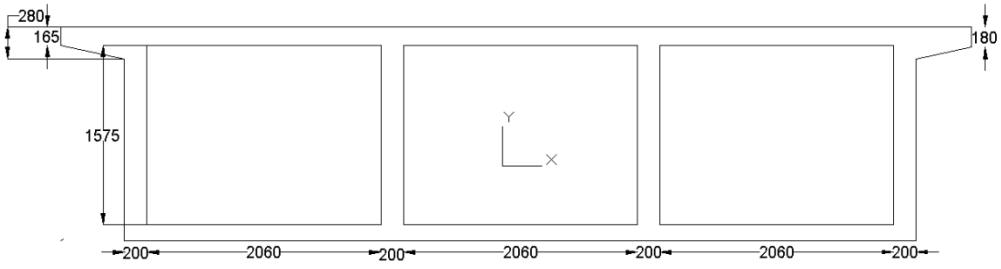

ALL Units are in mm.
Hollow Concrete Section for Bridge Girder
Please note that the dimensions of flanges on either side are different

(c) Girder Sections

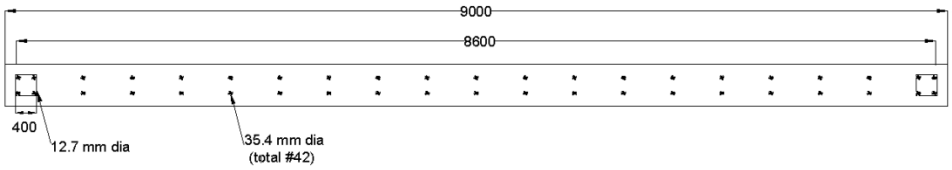

(d) Cross section of Bent 9

Figure 1 **:** (a) Schematic diagram of the test-bed bridge, (b) girder sections, (c) cross sections of the piers, (d) cross section of bent 9

3.1. Bridge modeling and validation

3.1.1 Modeling of bridge components

Finite element analyses (FEAs) of the bridge is performed under the Northridge earthquake ground motions recoded at the nearest station to the bridge. Modeling of various bridge components and their geometric and material properties are discussed next.

Bridge girder – 140.4 m long bridge girder is modeled using linear elastic beam-column elements as is component is expected to respond within the elastic range during earthquakes. The beam-column elements are aligned along the center line of the bridge deck. To obtain properties of bridge girder, the cross-section of the girder is modeled in STAAD (Bentley Structures, STAADPro Section Designer, Yorba Linda, CA, 2011) and obtained properties are summarized in Table 2

Table 2:Cross-sectional properties of girder section

Area	3625050.23 mm^2	Section Modulus –x	1.92 x 10^9 mm^3
Torsional Constant	5.32 x 10^{12} mm^4	Section Modulus – y	5.01 x 10^9 mm^3
Moment of Inertia – x	1.98 x 10^{12} mm^4	Pl Section Modulus – x	2.5 x 10^9 mm^3
Moment of Inertia – y	1.99 x 10^{13} mm^4	Pl Section Modulus – y	7.44 x 10^9 mm^3
Shear Area – x	9.84 x 10^5 mm^2	Rad of Gyration – x	740.06 mm
Shear Area – y	2.65 x 10^5 mm^2	Rad of Gyration – y	2347.95 mm

Bridge piers – During seismic excitation, the maximum bending moment generates at pier ends. This often leads to the formation of plastic hinges at these locations when the generated moment exceeds the plastic moment capacity of these sections. To model such nonlinear behavior at bridge pier ends, nonlinear rotational springs are introduced in bridge models at the top and bottom of each pier. Rigid elements are assigned at pier ends (i.e., at pier-girder and pier-foundation connections). This ensures rigid connectivity at pier-girder connections of monolithic concrete bridges. The length of the plastic hinge L_p (inch) through which plastic moment M_P generates is calculated as

$$L_P = 0.08L + 0.15F_{ye}d_{bl} \quad (7)$$

where, L_P is the distance from the critical section of the plastic hinge to the point of contraflexure (inch), F_{ye} is design yield strength (ksi) for the longitudinal bars in the

plastic hinge region and d_{bl} is the diameter (inch) of the longitudinal reinforcement. These values can be seen in Table 3.

Table 3: Plastic hinge lengths and axial loads

Bridge Pier	Bent 5	Bent 6	Bent 7	Bent 8	Bent 9
Length of Plastic Hinge ft (mm)	2.07(631)	2.07(631)	2.52(768)	2.07(631)	2.35(717)
Load(Kips)	504	489	537	605	560

The cap beam for bent 5 is modeled as a rigid link (Nielson and Desroches 2007). Figure 2 shows the actual and bi-linear moment-rotation envelopes of bridge piers that are developed through the moment-curvature analysis described in Priestley *et al*. (1996). In these figures, M_y and M_u represent the yield and ultimate moment carrying capacities of pier cross-sections, respectively, and M_y and M_u are corresponding rotations. $K_{elastic}$ represents the initial elastic stiffness of the member and α_{PY} is the post yield stiffness ratio. Axial load levels (Table 3) on these piers vary from one pier to the other, and hence, moment curvature relations from bents 6, 7 and 8 are different although they have the same cross-sections. For bent 9, the moment curvature plots are different in the longitudinal and transverse direction of the bridge. As expected, moment rotation relation in the transverse direction is much stronger than the longitudinal direction.

Values of elastic stiffness, yield strength and post-yield stiffness ratio for all Piers 5 to 9 are summarized in Table 4.

Table 4: Stiffness, moment capacity and stiffness ratio of the bridge piers

Bridge Pier	Elastic Stiffness	Yield Strength	Post Yield Stiffness Ratio
Bent 5	1.125 e6 kips /ft	1602 kips-ft	0.0181
Bent 6	2.995e6 kips /ft	5304 kips-ft	0.0138
Bent 7	2.4e6 kips /ft	5376 kips-ft	0.013
Bent 8	3.021e6 kips /ft	5442kips-ft	0.0119
Bent 9 - Transverse	1.9e8 kips /ft	46720 kips-ft	0.03
Bent 9 - Longitudinal	5.6e5 kips /ft	1934kips-ft	0.005

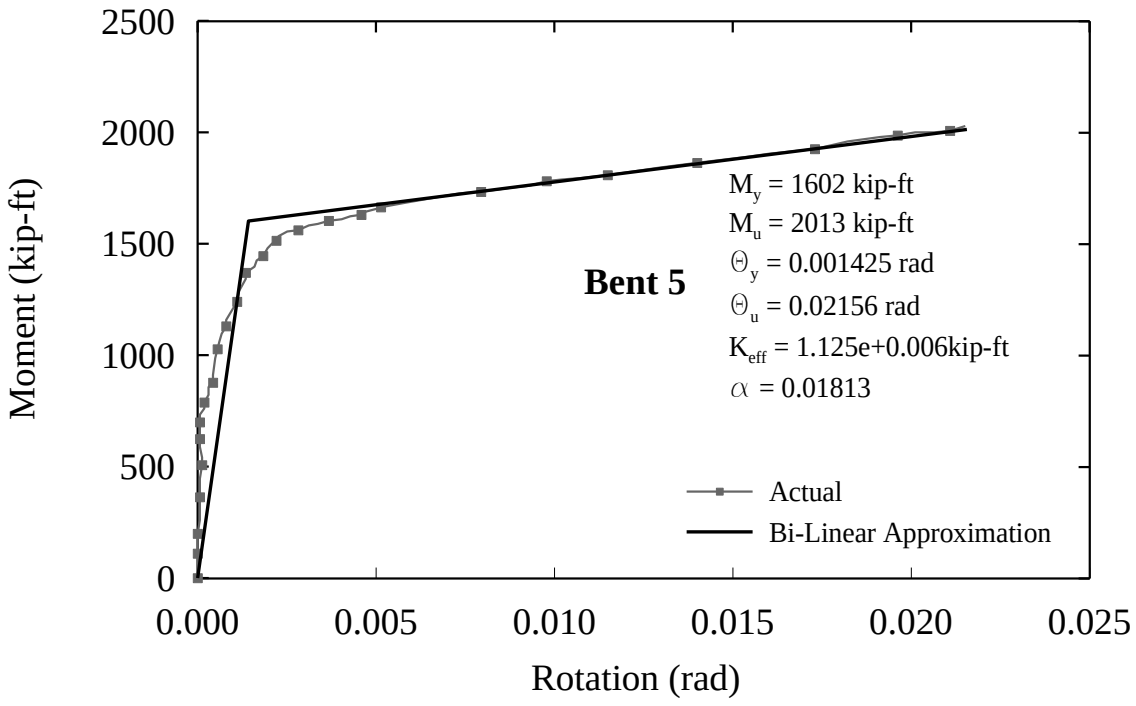
Moment (kip-ft)
Rotation (rad)
Bent 5
M_y = 1602 kip-ft
M_u = 2013 kip-ft
Θ_y = 0.001425 rad
Θ_u = 0.02156 rad
K_{eff} = 1.125e+0.006kip-ft
α = 0.01813
Actual
Bi-Linear Approximation
0
500
1000
1500
2000
2500
0.000
0.005
0.010
0.015
0.020
0.025

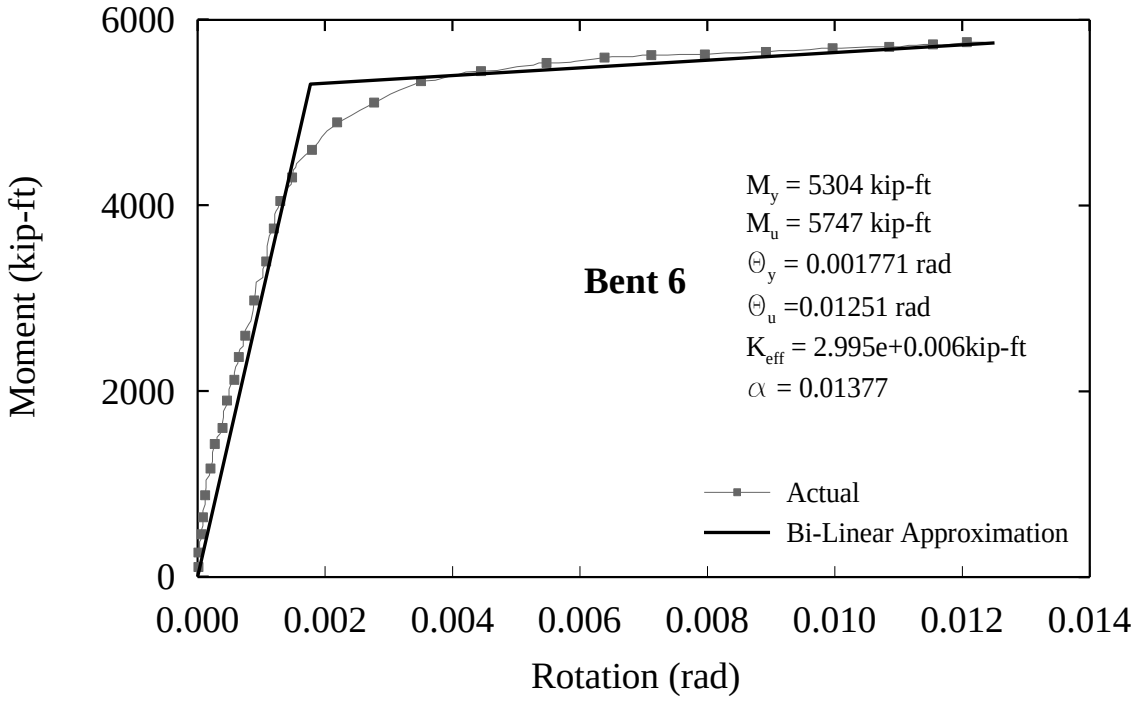
Moment (kip-ft)
Rotation (rad)
Bent 6
M_y = 5304 kip-ft
M_u = 5747 kip-ft
Θ_y = 0.001771 rad
Θ_u =0.01251 rad
K_{eff} = 2.995e+0.006kip-ft
α = 0.01377
Actual
Bi-Linear Approximation
0
2000
4000
6000
0.000
0.002
0.004
0.006
0.008
0.010
0.012
0.014

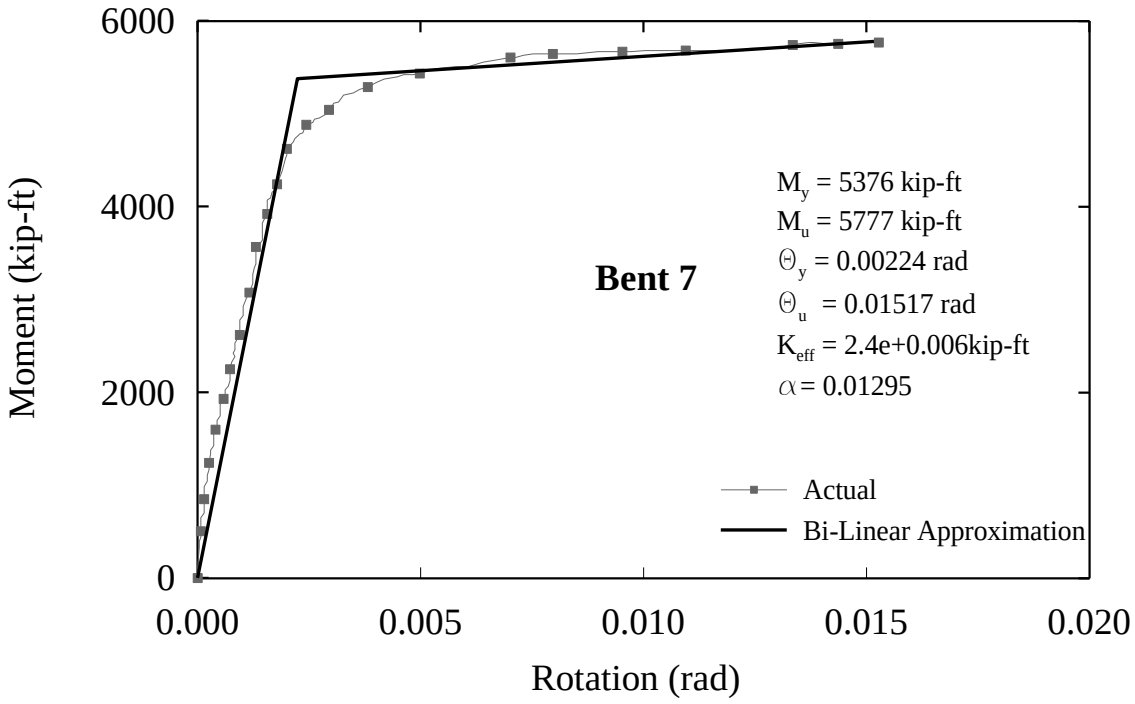
Moment (kip-ft)
6000
4000
2000
0
0.000
0.005
0.010
0.015
0.020
Rotation (rad)
Bent 7
My = 5376 kip-ft
Mu = 5777 kip-ft
Θy = 0.00224 rad
Θu = 0.01517 rad
Keff = 2.4e+0.006kip-ft
α = 0.01295
Actual
Bi-Linear Approximation

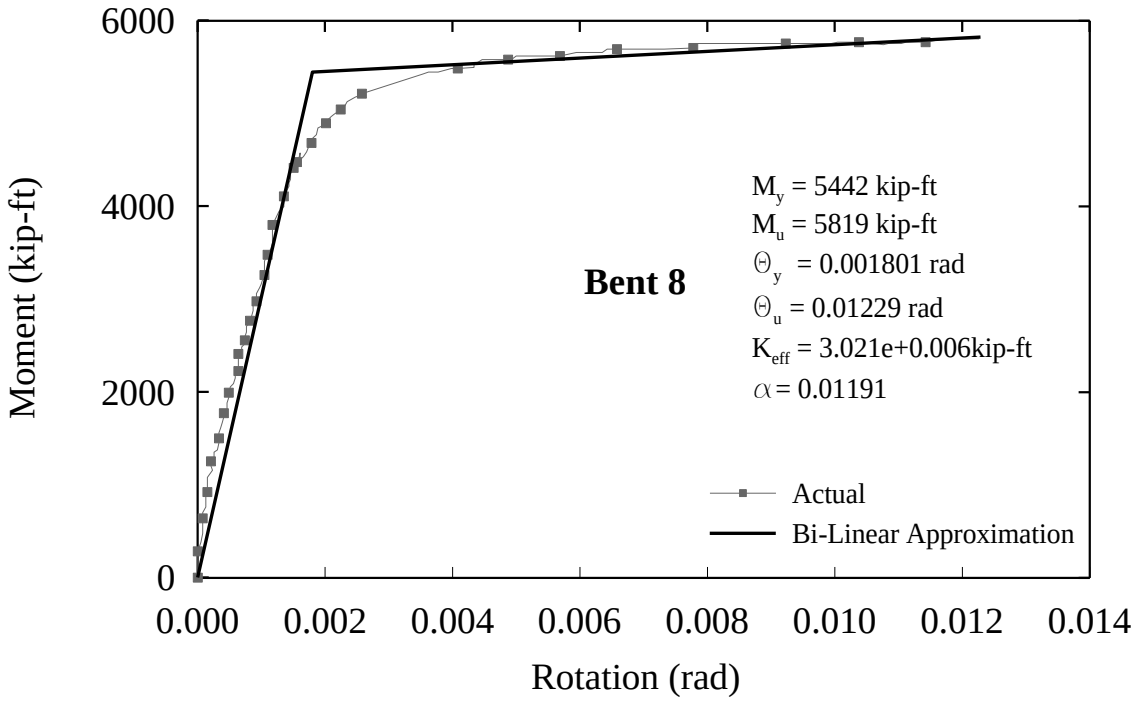
Moment (kip-ft)
6000
4000
2000
0
0.000
0.002
0.004
0.006
0.008
0.010
0.012
0.014
Rotation (rad)
Bent 8
My = 5442 kip-ft
Mu = 5819 kip-ft
Θy = 0.001801 rad
Θu = 0.01229 rad
Keff = 3.021e+0.006kip-ft
α = 0.01191
Actual
Bi-Linear Approximation

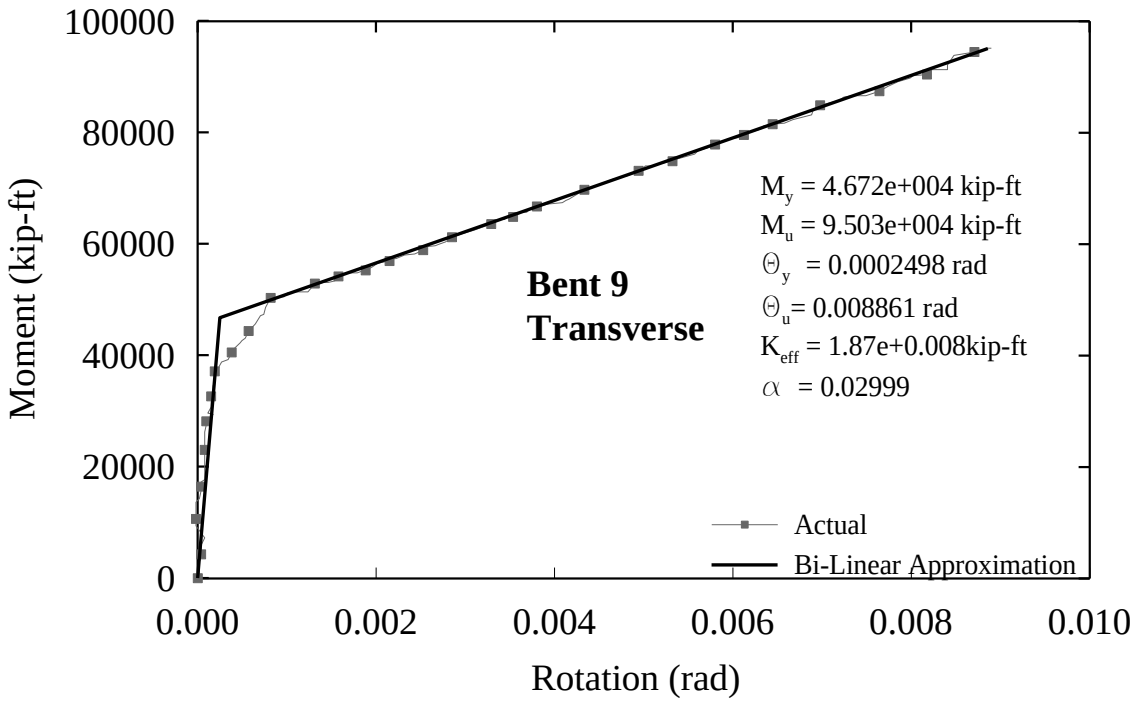

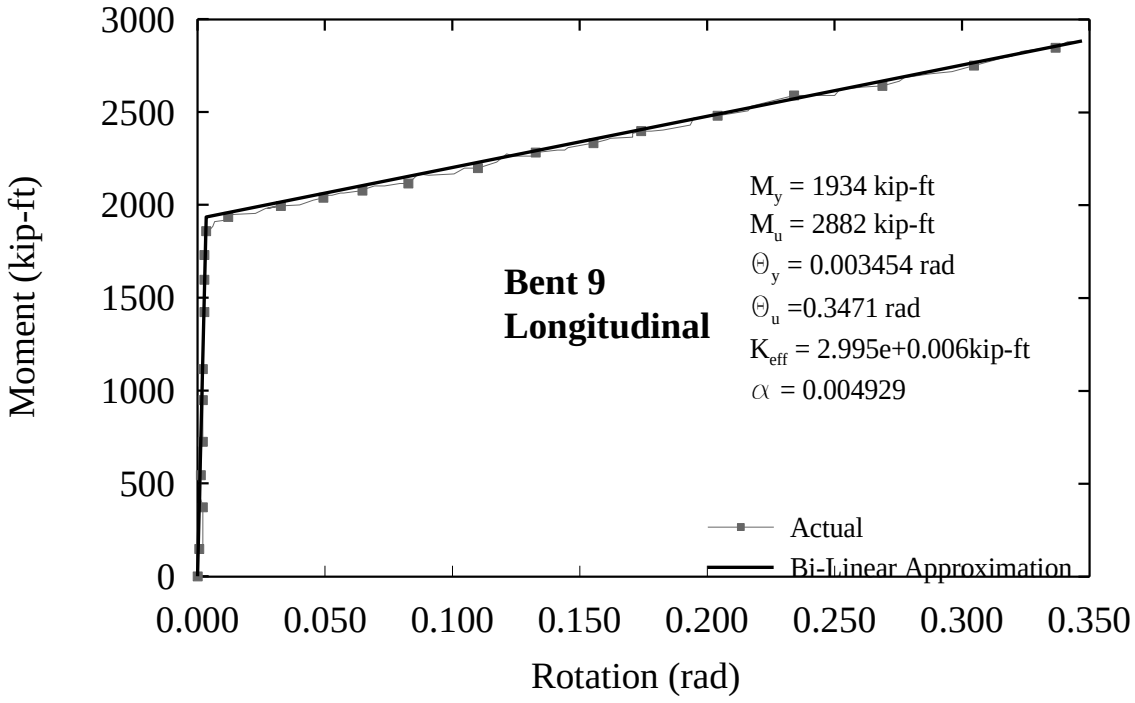

Figure 2: Moment rotation diagrams for bents 5 to 9

In span expansion joint - At in-span expansion joint, the bridge is modeled such that the two ends of expansion joint can move independently in the longitudinal direction and rotate in longitudinal plane while they have no relative vertical movement. During out-of-plane motion, they are assumed to have a pin connection. The opening and closure of expansion joints during bridge movement are modeled by assigning hook and gap elements, respectively. The hook element represents the effect of restrainer at expansion joint and controls relative displacement (excessive separation) between two adjacent girders at the expansion joint. A non-linear link element RESTR with an initial slack of 25.4mm is used as a hook element. Therefore, force develops in RESTR element when the outward relative displacement of adjacent bridge decks is more than initial slack. A nonlinear gap element with an initial gap of 12.7mm and linear elastic stiffness of 223292 KN/m (calculated according to Cofer *et al*., 1997) for longitudinal translation are assigned. Hence, the gap element becomes active only when the relative inward displacement of adjacent bridge decks in the longitudinal direction of the bridge exceeds the initially provided gap width of 12.7 mm. The gap properties used for the present study are summarized in Table 5.

Table 5: Properties of GAP element

Link Name	Type	Gap Width	DOF	Stiffness
GAP	Non-Linear Link	12.7 mm	U1	223292 KN/m

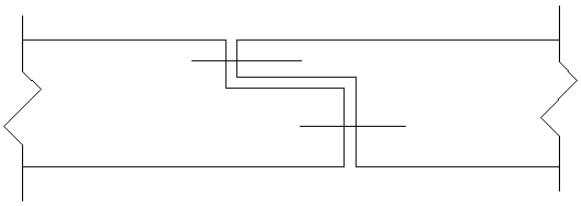

(a)

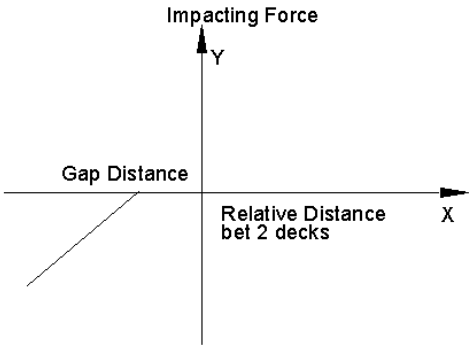

(b)

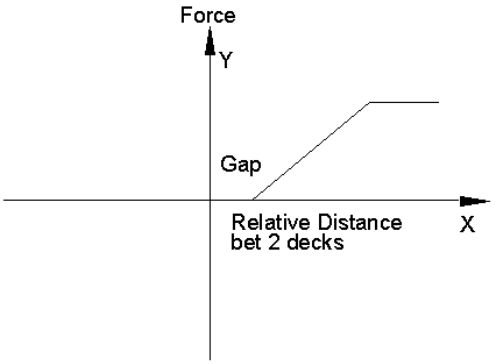

(c)

Figure 3: (a) Schematic Diagram of expansion joint, (b) function of gap element and (c) function of restrainer element

Foundation – The Bridge is located on the site of an old river-bed. Therefore, stiffness of bridge foundation should be calculated according to the local site profile. For the model validation purpose, the present study develops a finite element model of the bridge with fixed-base condition. Once validated, appropriate foundation model is assigned to realistically capture the soil-foundation interaction.

3.1.2. Northridge earthquake ground motions records

Broderick and Elnashai (1994) analyzed the nonlinear response of the bridge under the Northridge earthquake and made a qualitative comparison of the bridge response observed during that earthquake. The results presented in this literature are used in the present study to validate the bridge model. For this purpose, consistency is maintained in assigning boundary conditions of the bridge at foundations. The bridge is analyzed under the ground motions recorded during the Northridge Earthquake, 1994.

To validate the bridge model, bridge response from nonlinear time history analysis will be compared with that presented in. This literature simulated damage of the bridge due to the 1994 Northridge earthquake. Ground motion components of this earthquake were recorded at the City Hall stations in Santa Monica, approximately 10 km from the bridge site. This is the nearest recording station amongst several others located in this region. Peak ground accelerations (PGAs) of these acceleration records are 0.370g, 0.883g and 0.230g respectively for longitudinal, transverse and vertical components of the motion. Figure 4 shows complete time histories of recorded motions in the

longitudinal and transverse directions of the bridge respectively. These motions are obtained from Pacific Earthquake Engineering Research (PEER) strong motion database.

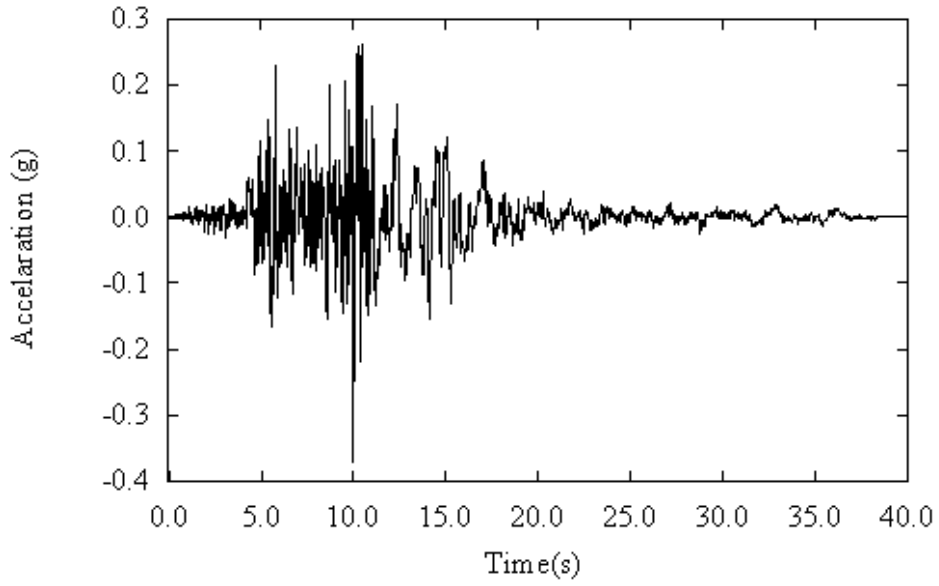

Longitudinal ground motion

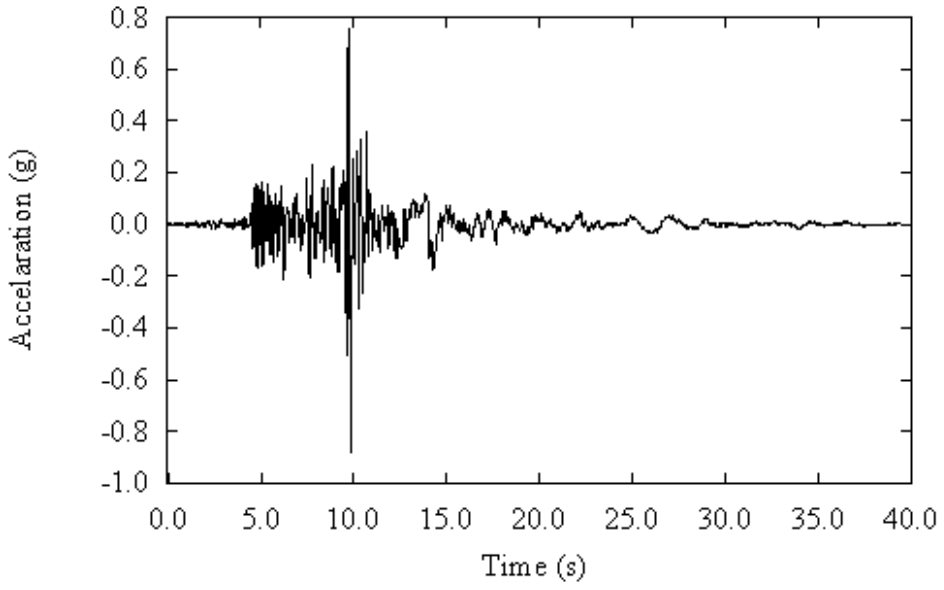

Transverse ground motion

Figure 4: Longitudinal and transverse ground motions recorded near site

3.1.3. Bridge response under the Northridge earthquake and model validation

Fundamental time periods and mode shapes of the bridge at the first five modes are compared with results from Broderick and Elnashai (1994) and presented in Table 7. As can be seen from this table, values obtained in this study from the numerical model are in well agreement with that calculated in the previous research. Table 8 shows shear capacities of the bridge at pier 6, 7 and 8 and developed shear forces at the same locations obtained from time history analysis under the simultaneous application of two horizontal components of Northridge earthquake. Shear capacities at bridge piers are calculated following Priestley et al. (1996) using Eq. (8) to (11). Reduction factors for shear area and moment of inertia are calculated from Priestley *et al.* (1996), the reduction factor for torsional rigidity is taken as 0.2 following the recommendations of Aviram *et al*. (2008). These are reported in Table 6. Developed shear forces at bridge piers represents shear demands from this seismic event; these values are the maximum shear forces recorded at these locations throughout the time history analysis of the bridge. Comparison of shear capacity and demand shows that pier 6 fails in shear as the demand exceeds capacity at this location. The same phenomenon is also observed in real-life. During the Northridge earthquake, the bridge failed due to the shear failure of pier 6. A similar observation is also found in Broderick and Elnashai (1994). Hence, these comparisons confirm the validity of the numerical bridge model developed here.

Table 6: Reduction factors for effective section properties

Member	Cross Sectional Area	Shear Area	Moment of Inertia	Torsional Rigidity
Bent 5	0.28	0.28	0.28	0.2
Bent 6	1	0.68	0.68	0.2
Bent 7	1	0.68	0.68	0.2
Bent 8	1	0.68	0.68	0.2
Bent 9	1	0.28	0.28	0.2
Girder	1	1	0.75	0.2

$$V_n = V_c + V_s + V_p \tag{8}$$

where,

$$V_c = k\sqrt{f'_c}A_e \tag{9}$$

$$V_s = \frac{A_h f_{yh} D' \cot\theta}{s} \quad \text{(circular columns)}$$

$$V_s = \frac{A_v f_y D' \cot\theta}{s} \quad \text{(rectangular columns)} \tag{10}$$

$$V_p = P\tan\alpha \tag{11}$$

In Eq. (8) which defines the contribution of concrete to the shear strength, the effective shear area $A_e = 0.8\,A_{gross}$, and k is a function of the ductility factor μ. In Eq. (9)

which defines the contribution of steel to shear strength, A_h is the area of the transverse reinforcement, *D'* is a cross-sectional property and the angle θ may be taken as 30 degrees unless the corner-to-corner diagonal of the member subtends a larger angle with the member axis, in which case the larger angle is used. In Eq. (10) the angle α is a geometric property and it defines the contribution of the axial force to the shear strength.

Table 7: Comparison of modal shapes and time periods

Values from Model		Values from Paper	
0.44	Transverse	0.46	Transverse
0.29	Transverse	0.28	Transverse
0.24	Deck	0.20	Deck
0.20	Deck	0.16	Deck
0.18	Deck	0.16	Deck
0.17	Transverse	0.11	Longitudinal

Table 8: Comparison of developed shear forces and shear capacities of bridge piers

Location of the bridge	Shear Force	Shear Capacity	Conclusion
Pier 6	2540 KN	2537 KN	Pier 6 failed in shear
Pier 7	2063 KN	2353 KN	
Pier 8	2362 KN	2715 KN	

Chapter 4 Seismic Resilience of the bridge

Broderick and Elnashai (1994) applied fixed conditions at bridge pier bases. The same condition is considered in this study for the validation purpose. Post-validation, boundary conditions at pier bases of the test-bed bridge are revised to include the effect of foundation-soil interaction in bridge dynamic response. Type 'M' and 'H' piers were supported on groups of 14 and 12 piles of 400 mm diameter respectively. Foundation springs are assigned at pier bases based on the details available from Broderick and Elnashai (1994) and engineering judgment.

The spring constants are calculated according to the recommendations of Nielson and Desroches (2006) as 7 KN/mm/pile for lateral stiffness. The authors assumed these values for pile configurations from Caltrans 1999. The foundation joints are restrained in the vertical direction as the vertical stiffnesses are generally high. Owing to these high values, the rotational spring constants obtained are considerably high; hence the foundation joints are restrained for rotation. This resulted in a transverse stiffness of 98 KN/mm and 84 KN/mm for 'M' and 'H' type piers.

4.1. Bridge fragility curves

To develop fragility curves, time history analyses of the bridge is performed under sixty ground motions which were originally generated by the Federal Emergency Management Agency (FEMA) for the Los Angeles region in California (http://nisee.berkeley.edu/data/strong_motion/sacsteel/ground_motions.html). These ground motions include both recorded and synthetic motions and are categorized into three sets having annual exceedance probabilities of 2%, 10% and 50% in 50 years. Each set has 20 ground motions; LA01 to LA20 represent moderate motions with annual exceedance probability of 10% in 50 years, LA21 to LA40 represent strong motions with annual exceedance probability of 2% in 50 years, and LA41 to LA60 represent weak motions with annual exceedance probability of 50% in 50 years. This wide range of seismic hazards covered through these motions is preferable for seismic fragility analysis of the bridge. Table 9 shows the range of PGA values of the ground motions under each of these three sets.

Table 9: PGA values of LA ground motions having various hazard levels

Los Angeles Ground motions having a Probability of Exceedance of 10% in 50 year

SAC Name	Record	Earthquake Magnitude	Distance (km)	Scale Factor	Number of Points	DT (sec)	Duration (sec)	PGA (cm/sec2)
LA01	Imperial Valley, 1940, El Centro	6.9	10	2.01	2674	0.02	39.38	452.03
LA02	Imperial Valley, 1940, El Centro	6.9	10	2.01	2674	0.02	39.38	662.88
LA03	Imperial Valley, 1979, Array #05	6.5	4.1	1.01	3939	0.01	39.38	386.04
LA04	Imperial Valley, 1979, Array #05	6.5	4.1	1.01	3939	0.01	39.38	478.65
LA05	Imperial Valley, 1979, Array #06	6.5	1.2	0.84	3909	0.01	39.08	295.69
LA06	Imperial Valley, 1979, Array #06	6.5	1.2	0.84	3909	0.01	39.08	230.08
LA07	Landers, 1992, Barstow	7.3	36	3.2	4000	0.02	79.98	412.98
LA08	Landers, 1992, Barstow	7.3	36	3.2	4000	0.02	79.98	417.49
LA09	Landers, 1992, Yermo	7.3	25	2.17	4000	0.02	79.98	509.7
LA10	Landers, 1992, Yermo	7.3	25	2.17	4000	0.02	79.98	353.35

LA11	Loma Prieta, 1989, Gilroy	7	12	1.79	2000	0.02	39.98	652.49
LA12	Loma Prieta, 1989, Gilroy	7	12	1.79	2000	0.02	39.98	950.93
LA13	Northridge, 1994, Newhall	6.7	6.7	1.03	3000	0.02	59.98	664.93
LA14	Northridge, 1994, Newhall	6.7	6.7	1.03	3000	0.02	59.98	644.49
LA15	Northridge, 1994, Rinaldi RS	6.7	7.5	0.79	2990	0.005	14.945	523.3
LA16	Northridge, 1994, Rinaldi RS	6.7	7.5	0.79	2990	0.005	14.945	568.58
LA17	Northridge, 1994, Sylmar	6.7	6.4	0.99	3000	0.02	59.98	558.43
LA18	Northridge, 1994, Sylmar	6.7	6.4	0.99	3000	0.02	59.98	801.44
LA19	North Palm Springs, 1986	6	6.7	2.97	3000	0.02	59.98	999.43
LA20	North Palm Springs, 1986	6	6.7	2.97	3000	0.02	59.98	967.61

Los Angeles Ground motions having a Probability of Exceedance of 2% in 50 years

SAC Name	Record	Earthquake Magnitude	Distance (km)	Scale Factor	N0. of Points	DT sec	Duration (sec)	PGA (cm/sec^2)
LA21	1995 Kobe	6.9	3.4	1.15	3000	0.02	59.98	1258
LA22	1995 Kobe	6.9	3.4	1.15	3000	0.02	59.98	902.75
LA23	1989 Loma Prieta	7	3.5	0.82	2500	0.01	24.99	409.95
LA24	1989 Loma Prieta	7	3.5	0.82	2500	0.01	24.99	463.76
LA25	1994 Northridge	6.7	7.5	1.29	2990	0.005	14.945	851.62
LA26	1994 Northridge	6.7	7.5	1.29	2990	0.005	14.945	925.29
LA27	1994 Northridge	6.7	6.4	1.61	3000	0.02	59.98	908.7
LA28	1994 Northridge	6.7	6.4	1.61	3000	0.02	59.98	1304.1
LA29	1974 Tabas	7.4	1.2	1.08	2500	0.02	49.98	793.45
LA30	1974 Tabas	7.4	1.2	1.08	2500	0.02	49.98	972.58
LA31	Elysian Park (simulated)	7.1	17.5	1.43	3000	0.01	29.99	1271.2
LA32	Elysian Park (simulated)	7.1	17.5	1.43	3000	0.01	29.99	1163.5
LA33	Elysian Park (simulated)	7.1	10.7	0.97	3000	0.01	29.99	767.26
LA34	Elysian Park (simulated)	7.1	10.7	0.97	3000	0.01	29.99	667.59
LA35	Elysian Park (simulated)	7.1	11.2	1.1	3000	0.01	29.99	973.16
LA36	Elysian Park (simulated)	7.1	11.2	1.1	3000	0.01	29.99	1079.3
LA37	PaloVerdes (simulated)	7.1	1.5	0.9	3000	0.02	59.98	697.84

LA38	Palos Verdes (simulated)	7.1	1.5	0.9	3000	0.02	59.98	761.31
LA39	Palos Verdes (simulated)	7.1	1.5	0.88	3000	0.02	59.98	490.58
LA40	Palos Verdes (simulated)	7.1	1.5	0.88	3000	0.02	59.98	613.28

Los Angeles Ground motions having a Probability of Exceedance of 50% in 50 years

SAC Name	Record	Earthquake Magnitude	Distance (km)	Scale Facor	Number of Points	DT (sec)	Duration (sec)	PGA (cm/sec2)
LA41	Coyote Lake, 1979	5.7	8.8	2.28	2686	0.01	39.38	578.34
LA42	Coyote Lake, 1979	5.7	8.8	2.28	2686	0.01	39.38	326.81
LA43	Imperial Valley, 1979	6.5	1.2	0.4	3909	0.01	39.08	140.67
LA44	Imperial Valley, 1979	6.5	1.2	0.4	3909	0.01	39.08	109.45
LA45	Kern, 1952	7.7	107	2.92	3931	0.02	78.6	141.49
LA46	Kern, 1952	7.7	107	2.92	3931	0.02	78.6	156.02
LA47	Landers, 1992	7.3	64	2.63	4000	0.02	79.98	331.22
LA48	Landers, 1992	7.3	64	2.63	4000	0.02	79.98	301.74
LA49	Morgan Hill, 1984	6.2	15	2.35	3000	0.02	59.98	312.41

LA50	Morgan Hill, 1984	6.2	15	2.35	3000	0.02	59.98	535.88
LA51	Parkfield, 1966, Cholame 5W	6.1	3.7	1.81	2197	0.02	43.92	765.65
LA52	Parkfield, 1966, Cholame 5W	6.1	3.7	1.81	2197	0.02	43.92	619.36
LA53	Parkfield, 1966, Cholame 8W	6.1	8	2.92	1308	0.02	26.14	680.01
LA54	Parkfield, 1966, Cholame 8W	6.1	8	2.92	1308	0.02	26.14	775.05
LA55	North Palm Springs, 1986	6	9.6	2.75	3000	0.02	59.98	507.58
LA56	North Palm Springs, 1986	6	9.6	2.75	3000	0.02	59.98	371.66
LA57	San Fernando, 1971	6.5	1	1.3	3974	0.02	79.46	248.14
LA58	San Fernando, 1971	6.5	1	1.3	3974	0.02	79.46	226.54
LA59	Whittier, 1987	6	17	3.62	2000	0.02	39.98	753.7
LA60	Whittier, 1987	6	17	3.62	2000	0.02	39.98	469.07

The test-bed bridge is most vulnerable in the transverse direction. During the Northridge earthquake, major horizontal ground motion component propagated along the transverse direction of the bridge resulting in shear failure in this direction. To be

consistent with the actual damage of the bridge, seismic fragility analysis is performed by applying LA ground motions in the transverse direction of the bridge. Bridge seismic damage is characterized through shear and flexural failures of bridge piers. These two failure modes are assumed to govern the global failure of the bridge and other possible seismic bridge failure modes (such as unseating of bridge girders and failure at expansion joint) are assumed to be non-governing failure modes. In fact, the bridge is observed to have shear failure in real-life during the Northridge event. In general, shear failure of a bridge pier is brittle in nature and sometimes causes irreversible damage to bridges. Hence, such a mode of failure is considered here as ultimate damage (i.e., complete collapse) of the bridge. For flexural damage of bridge piers, HAZUS (1999) provided five different bridge damage states namely no, minor (or slight), moderate, major (or extensive) damage and complete collapse. Among these, the complete collapse state is the ultimate damage state of the bridge and others are named according to the severity of bridge seismic damage without complete failure.

To generate fragility curves of the bridge, shear and flexural damage of the bridge are defined in a quantitative manner. Seismic damage states are ranked with k = 1 to 4 in which k = 1 represents minor damage and k = 4 represents complete collapse. If shear failure occurs due to j^{th} ground motion, the bridge is considered to have damage condition r_j = 1 at damage state k = 4 (see Eq. 4). For flexural damage, bridge damage condition (r_j = 0 or 1) at a particular damage state is defined based on rotational ductility of bridge piers. By definition, rotational ductility (μ_ϕ) is the ratio of rotation (ϕ) of bridge piers to

the yield rotation (ϕ_y) measured at the same location. During time history analyses of the bridge under 60 LA motions, rotational time histories are recoded at both top and bottom of all bridge piers where plastic hinges are likely to appear. Rotational ductility for each pier is obtained by dividing maximum rotations from rotational time histories with yield rotations of corresponding locations that are obtainable from moment rotation plots shown in Figure 2. These rotational ductility values are considered as signature representing the flexural response of the bridge under seismic motions. To define damage condition of the bridge at each damage state and for each LA ground motion, rotational ductility values are compared with threshold limits. The bridge was constructed in 1964; so, it is reasonable to assume that bridge piers were not properly designed for seismic loading. The deficiency of lateral confinement in bridge piers was also evident in the post-Northridge reconnaissance report. Due to this reason, threshold limits of rotational ductility for various seismic damage states of the bridge are calculated based on drift limits of non-seismically designed bridge piers recommended in HAZUS (1999). Table 10 represents non-seismic drift limit ratios and threshold rotational ductilities of piers in Bent 6, 7 and 8 at different damage states. Note that the rotational ductility of the bridge at no damage state is always equal to 1.0 (= ϕ_y/ϕ_y), whereas the same for complete collapse state (= ϕ_u/ϕ_y; ϕ_u being ultimate rotation of bridge piers) varies from pier to pier. Hence, threshold rotational ductility for intermediate damage states (i.e., minor, moderate and major) also vary from pier to pier. Piers 5 and 9 are excluded from this table because it has a very high value of ultimate rotational ductility which indicates very low probability of forming plastic hinge in this pier resulting in

global failure of the bridge. Also, the shear forces developed in these piers were low relative to their shear capacities; hence they are excluded from shear comparisons as well.

Table 10: Drift ratios and corresponding values of ductility

Damage states	Non-seismic drift ratio (HAZUS 1999)	Threshold rotation ductility of bridge piers		
		Bent 6	Bent 7	Bent 8
No Damage	0.002	1	1	1
Minor	0.005	1.37	1.36	1.36
Moderate	0.01	2.01	1.96	1.97
Major	0.02	3.28	3.16	3.18
Collapse	0.05	7.06	6.77	6.82

Rotational ductilities of bridge piers are compared with threshold limits for all damage states and for each LA ground motion and damage conditions are assigned. Figure 5 shows the seismic fragility curves for the bridge at the minor, moderate, major damage and complete collapse states. For each fragility curve, standard deviation is kept constant (=0.5) to avoid intersection between any two fragility curves. Median values for all damage states are reported in the figure. Note that higher median value indicates less probability of bridge damage in a certain damage state. These fragility curves predict failure probabilities of the bridge in minor, moderate, major damage and complete collapse state are to be 100%, 99.7%, 95.3%, and 93.5%, respectively, under the transverse component of the Northridge earthquake (with PGA of 0.883g).

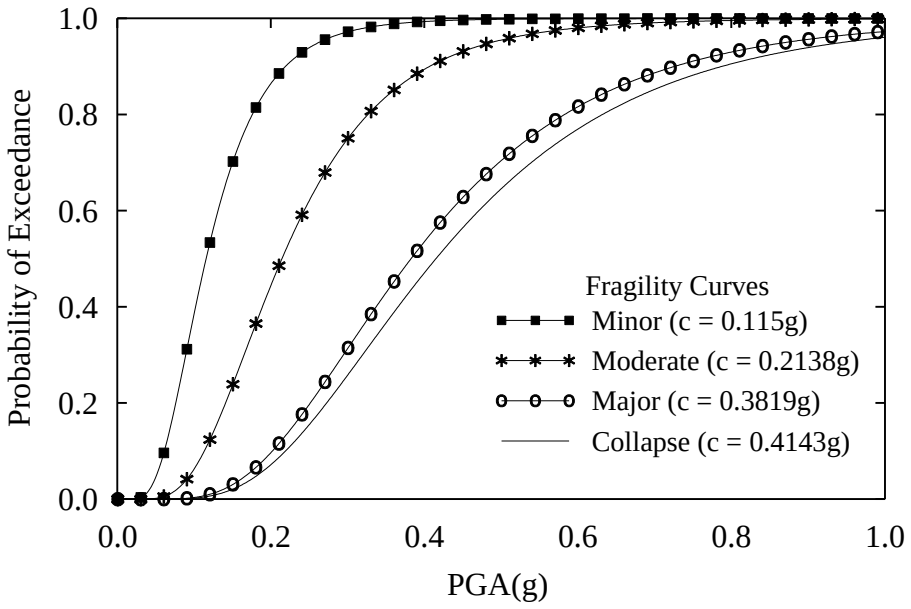

Figure 5: Fragility curves for the 4 different damage states

4.2. Direct and indirect losses due to the Northridge earthquake

The direct loss ratio is calculated as per the aforementioned loss function, the damage ratios for the different damage states are obtained from HAZUS (1999) and are listed in Table 11.

Table 11: Damage ratios for highway bridge components

Damage State	Damage ratio
Minor	0.03
Moderate	0.08
Extensive	0.25
Collapse	2/n , n:number of spans of bridge

These ratios are used to obtain the direct loss ratio for the bridge. For this study, the ratio of indirect losses to direct losses is assumed to be 13 from Denneman (2009). This ratio is used in Eq. (5) coupled with failure probabilities obtained for the ground motion at the City Hall stations in Santa Monica, approximately 10 km from the bridge site during the Northridge earthquake (1994). These probabilities are obtained from Figure 4 as a result of a fragility analysis. This resulted in an overall cost-ratio of 0.96, that was used in the resilience model to obtain the seismic resilience of the bridge.

The direct to indirect loss ratio is varied as part of a Sensitivity study to analyze the difference in values of resilience.

4.3. Post-event seismic recovery

As previously mentioned, it is very difficult to develop a closed-form mathematical expression for the post-earthquake recovery process. The present study considers three recovery models, linear, exponential and trigonometric (Cimellaro., 2008), to observed the influence of these models on seismic resilience of the bridge. Time required for complete recovery at various damage states are taken from HAZUS (1999) and given in Table 1. Using the above models for various parameters, a percentage value of resilience for the as-built bridge is computed as 57.47%. It is compared with the resilience of the bridge post-retrofit in Section 5.4 (Table 14).

$$f_{rec}(t,T_{RE}) = (1-\frac{t-t_{oe}}{T_{RE}}) \tag{12}$$

Eq. 12 shows the behavior of the linear recovery function; this is the simplest form of a recovery function that is generally used when there is no information regarding the preparedness, resources available or the societal response.

There are other forms of the function such as exponential and trigonometric which is used based on information available. These functions are shown in Eq. (13) and Eq. (14) respectively.

$$f_{rec}(t) = exp[-(t - t_{oE}) * (ln200) / T_{RE}] \quad (13)$$

$$f_{rec}(t) = 0.5 * \{1 + cos[\pi(t - t_{oE}) / T_{RE}]\} \quad (14)$$

The percentage values of resilience using these functions were obtained to be 99.92 % and 57.69% respectively.

Chapter 5 Proposed Retrofit Techniques and Enhancement in Seismic Resilience

The as-built bridge failed in shear. Thus, three bridge retrofit strategies are selected here that may reduce the shear demand from bridge piers. These strategies are (i) application of steel jackets around bridge piers, (ii) assigning seat-type abutment at the east end of the bridge, and (iii) assigning shear keys in addition to the seat-type abutment at the east end of the bridge. These retrofit strategies are applied considering the pre-Northridge condition of the bridge, and for each application enhancement in bridge seismic resilience is calculated.

5.1. Steel Jacketing

Concrete piers may be encased in steel jackets to help overcome column deficiencies. Piers with inadequate transverse reinforcements have limited ductility capacities and low shear strengths. Steel jacketing has been used as a retrofit measure to enhance the flexural ductility, shear strength, or performance of lap splices in reinforced concrete bridge piers. Extensive proof-of-concept tests of steel jacketed bridge piers have been performed at the University of California, San Diego in the early 1990s. Till date several hundred bridges in the US have been retrofitted with this technology to enhance their seismic performance.

Steel jackets are typically A36 steel casings that are applied to bridge piers keeping a space of about 50.8 mm at the pier ends to prevent the jacket from bearing on adjacent members.

The jacket thickness is decided based on the design charts provided by Priestley *et al*. (1996) as functions of column longitudinal reinforcement ratio and axial load ratio. It is adequate to provide for confinement of the lap splices and enhanced flexural confinement, with a significant increase in ductility capacity. Due to jacketing, compressive strength and ultimate strain of confined concrete fibers increase to a considerable extent. The confined compressive strength of concrete, f'_{cc}, is estimated from Chai et al. (1991) as follows

$$f'_{cc} = f'_c \left(2.254\sqrt{1+\frac{7.94 f'_l}{f'_c}} - \frac{2 f'_l}{f'_c} - 1.254\right) \quad (15)$$

where $f'c$ is the unconfined compressive strength of concrete. The radial confining stress in the steel jacket at yield f'_l is given by

$$f'_l = \frac{2 f_{yj} t_j}{(D_j - 2t_j)} \quad (16)$$

and f_{yj} is the yield stress of the jacket, D_j is the jacket diameter, and t_j is the jacket thickness. The corresponding conservative estimate of ultimate concrete strain capacity, ε_{cu}, is estimated by following the FHWA manual for seismic retrofitting for highway structures (FHWA, 2006) as given below.

$$\varepsilon_{cu} = 0.004 + \frac{5.6 t_j f_{ys}}{D_j f_{cc}} \quad (17)$$

5.1.1. Moment Rotation plots

New moment rotation plots for the jacketed bridge piers are shown in Figure 6.

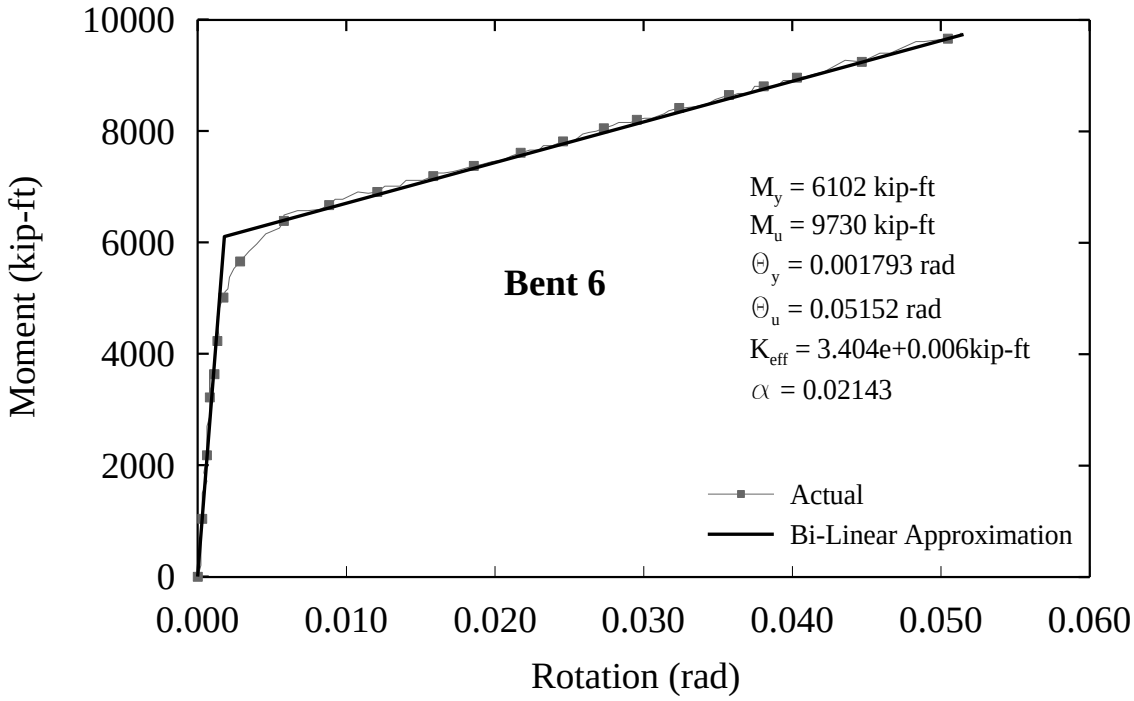

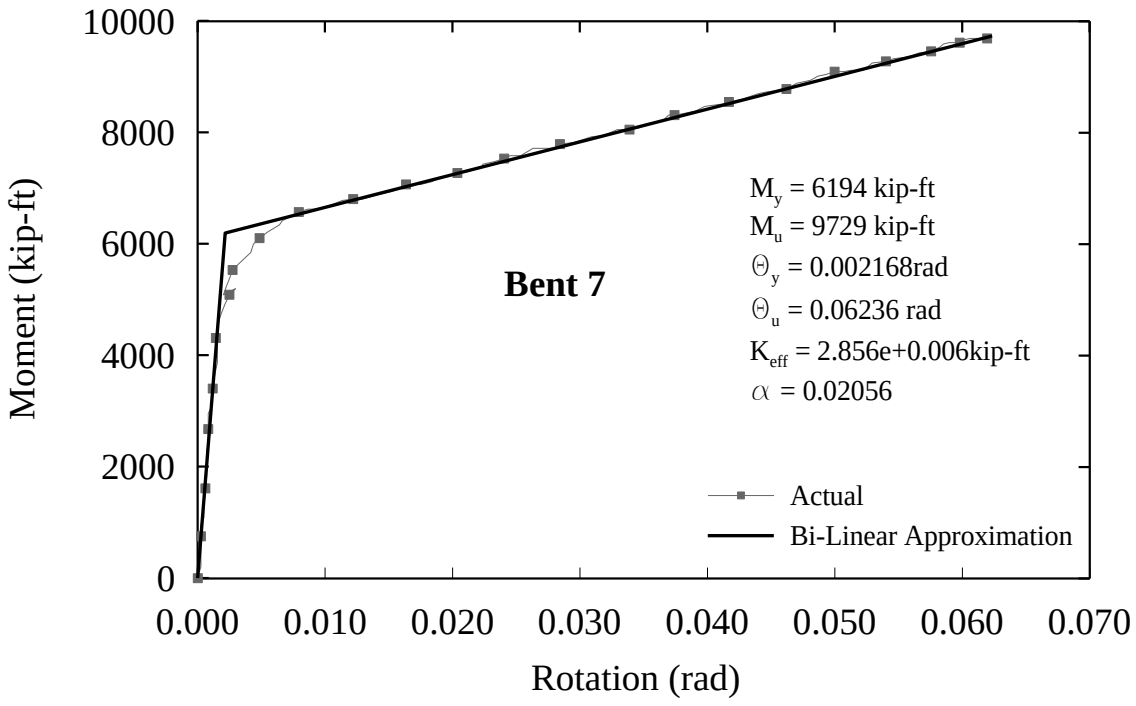

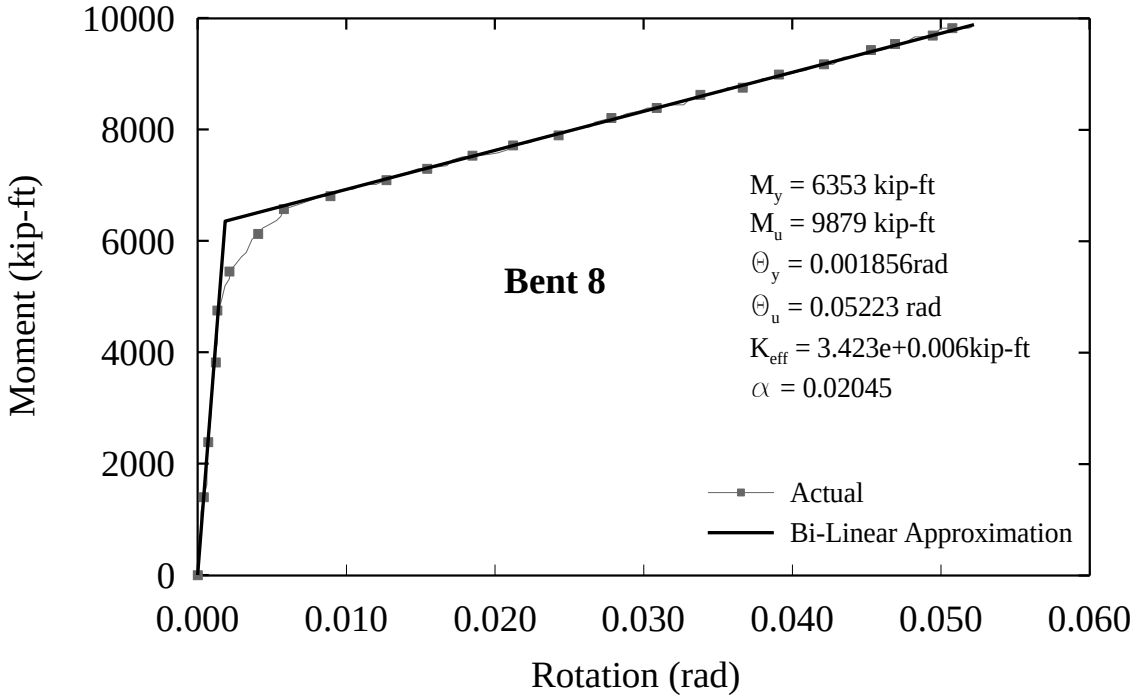

Figure 6: Moment rotation plots for retrofitted bents 6 to 8

5.1.2. Shear capacity of jacketed piers

Two potential methods are recognized to determine enhanced shear capacity of bridge piers after retrofitting these with steel jackets. For compassion purpose, shear capacity and seismic resilience of the retrofitted bridge are calculated using both of these methods.

According to FHWA (2006) recommendations, additional shear capacity V_{sj} provided by the jacket can be determined as

$$V_{sj} = \frac{\pi}{2} t f_{ys} D \cot\theta \tag{18}$$

where t is the thickness of the steel jacket, f_{ys} is the jacket yield stress and θ is the shear crack angle measured from the vertical plane.

The second method is given by Sakino *et al*. (2000) for determining shear capacity of square columns encased by steel jackets. The authors performed experiments to accurately assess the flexural response of retrofitted columns. A stress – strain model for confined concrete is developed based on the results obtained from this experiment and Eq. (19), a modified version of Ohno – Arakawa equation (AIJ, "Standard for Structural Calculation of Reinforced Concrete Structures," Architectural Institute of Japan, 1999), is proposed for determining the shear capacity of steel jacketed RC columns. Extending this recommendation to circular piers, the present study calculates shear capacity V_{sj} provided by steel jackets.

The total

$$V_{sj} = \{0.115 k_u . k_p \frac{17.65 + f'_c}{(a/D) + 0.12} + 0.85\sqrt{p_w f_{yt}} + 0.1\frac{N}{bD}\} bj(j = \frac{7}{8}d) \qquad (19)$$

where k_u = 1.0, $d<160$ mm

$1.19-0.012d$, 160 mm$<d<400$ mm

0.72, $d>400$ mm

$$kp = 0.82(100pt)^{0.23}$$

where,

k_u is the coefficient taking account for the scale effect, p_w is the reinforcement ratio of the transverse steel, b, D is the overall width and depth of the concrete section (mm), a/D is the shear span of column, N is the axial load applied (in KN), d is the effective depth of section (mm), p_t is the reinforcement ratio of the steel bars, f_{yt} is the yield Stress of jacket, B is the outside width of steel jacket and t is the thickness of steel jacket.

From the two methods, calculated shear capacities of bridge piers are given in Table 12. The shear capacity determined through the FHWA Recommendations largely depends on the ductility and is an envelope similar to the one discussed in Section 3.1.3

Table 12: Enhanced Shear Capacities for Piers 6 to 8

Method	Shear Capacity Pier 6	Shear Capacity Pier 7	Shear Capacity Pier 8
FHWA Recommendations	7640 KN	7547 KN	7901 KN
Ohno-Arakawa Equation	4210 KN	3609 KN	4218 KN

5.1.3. Fragility analysis of the retrofitted bridge

The retrofitted bridge is analyzed under 60 LA ground motions and for each motion, damage condition of the bridge is determined. Using the FHWA recommendations, the bridge observed minor damage state for 8 ground motions and it did not exceed the moderate damage state for any of the 60 ground motions. Using the Ohno-Arakawa equation for shear capacity, the bridge observed minor damage state for 8 ground motions and exceeded moderate damage state and experienced collapse for 7 out of those 8 ground motions.

Rotational ductilities of bridge piers are compared with threshold limits for all damage states (Table 13) and for each LA ground motion and damage conditions are assigned. Figure 7 shows the seismic fragility curves for the bridge at the minor, moderate, major damage and complete collapse states for shear capacity computed by the latter method.

For each fragility curve, standard deviation is kept constant (=0.5) to avoid intersection between any two fragility curves. The median values are included in the figure.

Table 13: Damage state ratios and corresponding values of ductility

Damage State	Non-seismic Ratio	Ductility Pier 6	Ductility Pier 7	Ductility Pier 8
No Damage	0.002	1	1	1
Minor	0.01	4.04	4.04	3.98
Moderate	0.025	9.74	9.75	9.57
Major	0.05	19.24	19.26	18.88
Collapse	0.075	28.73	28.76	28.19

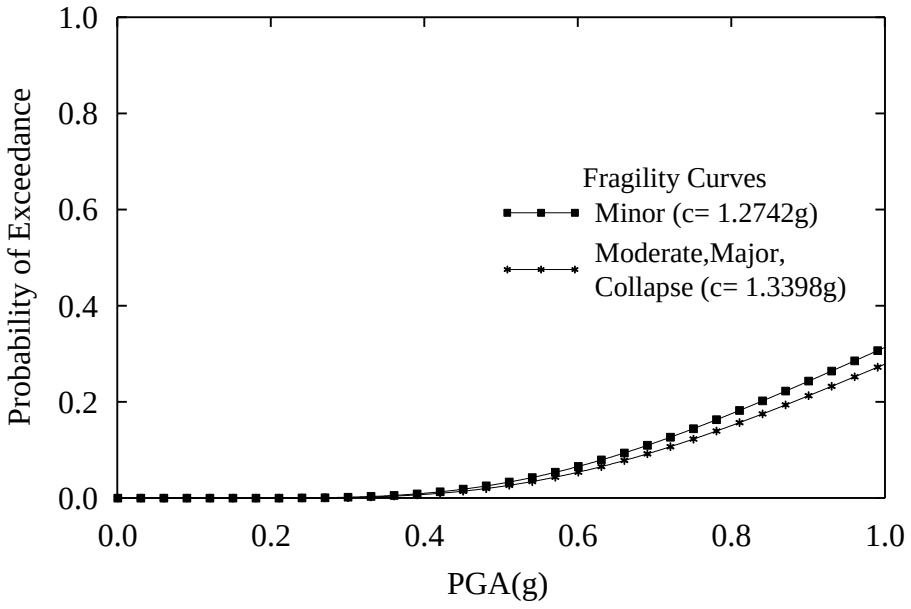

Figure 7: Fragility curves for the Retrofitted Structure (Ohno-Arakanawa Equation)

Figure 8 shows the seismic fragility curves for the bridge at the minor, moderate, major damage and complete collapse states for shear capacity computed by the latter method. The standard deviation is taken as a constant (= 0.5) and the median values are included in the figure. The fragility curve for the moderate and collapse damage state coincide with the x-axis in this case.

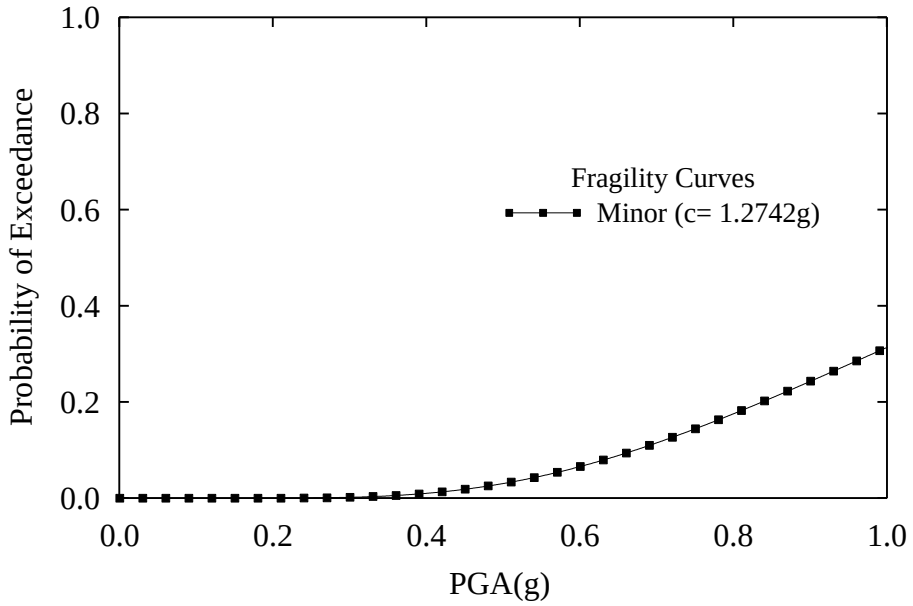

Figure 8: Fragility curves for the Retrofitted Structure (Seismic Retrofitting Manual)

The loss ratio when computed for the former case is found to be 0.09. The resulting loss ratio from the second method is computed according to the loss model and is found to be 0.69 including indirect losses. These values coupled with the linear recovery model using recovery times that commensurate to the dominating damage state (from Table 1) discussed are used to calculate resilience and are displayed in Table 14.

5.2. Abutment model

A moment release is assumed at the east abutment of the bridge. To study the effect of a traditional abutment in reducing the seismic shear demand at bridge piers, the east end of the bridge is modeled with seat-type abutment. Modeling of important components of a seat-type abutment (i.e., backwall and backfill, wingwall and bearing) are discussed in following sections.

5.2.1. Longitudinal Response due to backwall and backfill

During seismic motion, the passive resistance from the backfill soil is modeled following the recommendations of Caltrans (2004). This model includes effective abutment stiffness, K_{abut} that accounts for expansion gaps and incorporates a realistic value for the embankment fill response. The stiffness is adjusted proportional to the backwall/diaphragm height and is documented in Eq. 20. A gap of 2 inches is provided before the stiffness becomes active.

$$K_{abut} = K_i \times w \times \left(\frac{h}{1.7} \right) \tag{20}$$

where, w is the width of the backwall for the seat abutments and h is the height of the backwall element.

The passive pressure resisting the movement at the abutment shows a linear variation with the displacement as shown in Figure 9. The maximum passive pressure of 239 kPa,

presented in Eq. (21) is based on the ultimate static force developed in the full scale abutment testing conducted at UC Davis (Maroney, 1995).

$$P_{bw} = A_e \times (239kPa) \times \left(\frac{h_{bw}}{1.7} \right) \tag{21}$$

The effective area A_e for the seat type abutment is given by Eq. (22).

$$A_e = h_{bw} \times w_{bw} \tag{22}$$

w_{bw} and h_{bw} are taken as indicated in Figure 10.

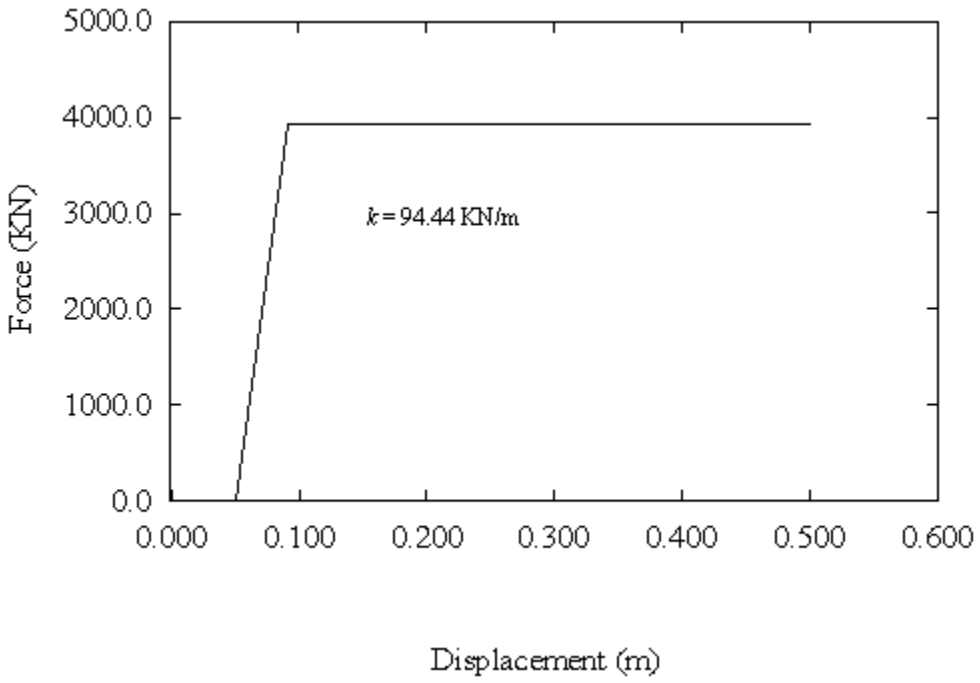

Figure 9: Force displacement response for Abutment Backfill

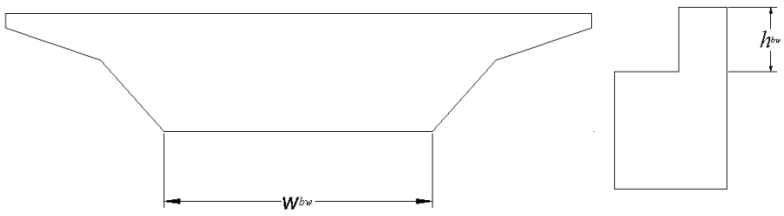

Figure 10: Effective area of cross-section

5.2.2. Longitudinal Response due to bearing

The authors attempt to include the behavior of an elastomeric bridge bearing in the longitudinal direction. They are very common bearings used on concrete girder bridges. They consist of an elastomeric rubber pad and steel dowels for restraint. A typical bearing size and configuration is used for this study from the recommendations of Nielson (2005), shown in Figure 11.

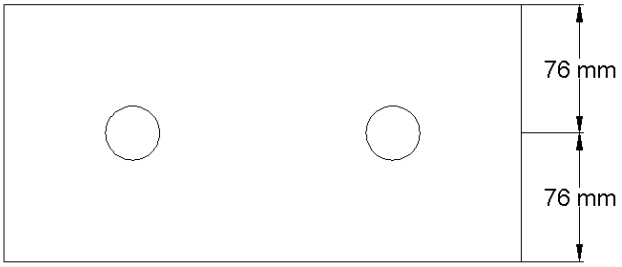

Figure 11: Typical elastomeric bearing

It consists of a neoprene pad that is 152 mm wide by 406 mm long and 25.4 mm thick. The behavior of this pad is characterized by sliding. There is an initial stiffness which continues to accept load until the coefficient of friction is exceeded, once it is exceeded, the stiffness changes to value that is zero. The pad is modeled as an elastic perfectly plastic material. The initial stiffness of the bearing is determined through Eq.23 (Kelly, 1997, Choi, 2002, Warn and Ryan, 2012).

$$k_0 = \frac{GA}{h} \tag{23}$$

where A is the area of the elastomeric bearing, G is the shear modulus of the elastomer and h is the thickness of the elastomeric pad. Shear values for elastomers in bridge bearings range between 0.66 MPa and 2.07 MPa depending on their hardness, an average value of 1.38 MPa is assumed for this study.

The frictional coefficient in the equation takes into account the friction between the concrete surface and the elastomeric rubber. Experimental tests show that the friction is a function of the normal stress on the bearing. For this study, this value is taken to be 0.36 which gives us an initial stiffness of 3.35 KN/mm. In the opening direction (i.e., when bridge girder moves away from the backwall) only the stiffness of bearing is active. When the gap is closed, abutment backwall is pushed towards the backfill and hence, resistance comes from backfill soil.

5.2.3. Transverse Response in wingwall

Transverse stiffness of abutments includes the contribution of wingwalls and the bearing discussed in the above section. Aviram et al. (2008) recommends the use of a modified backbone curve of longitudinal abutment stiffness to calculate abutment lateral resistance due to backfill, wing wall and pile systems. A wall modification factor of $C_L = 2/3$ and a participation coefficient of $C_w = 4/3$ is proposed in this literature following recommendations of Maroney and Chai (1994). Figure 12 shows wingwall dimensions the response curve used for the model.

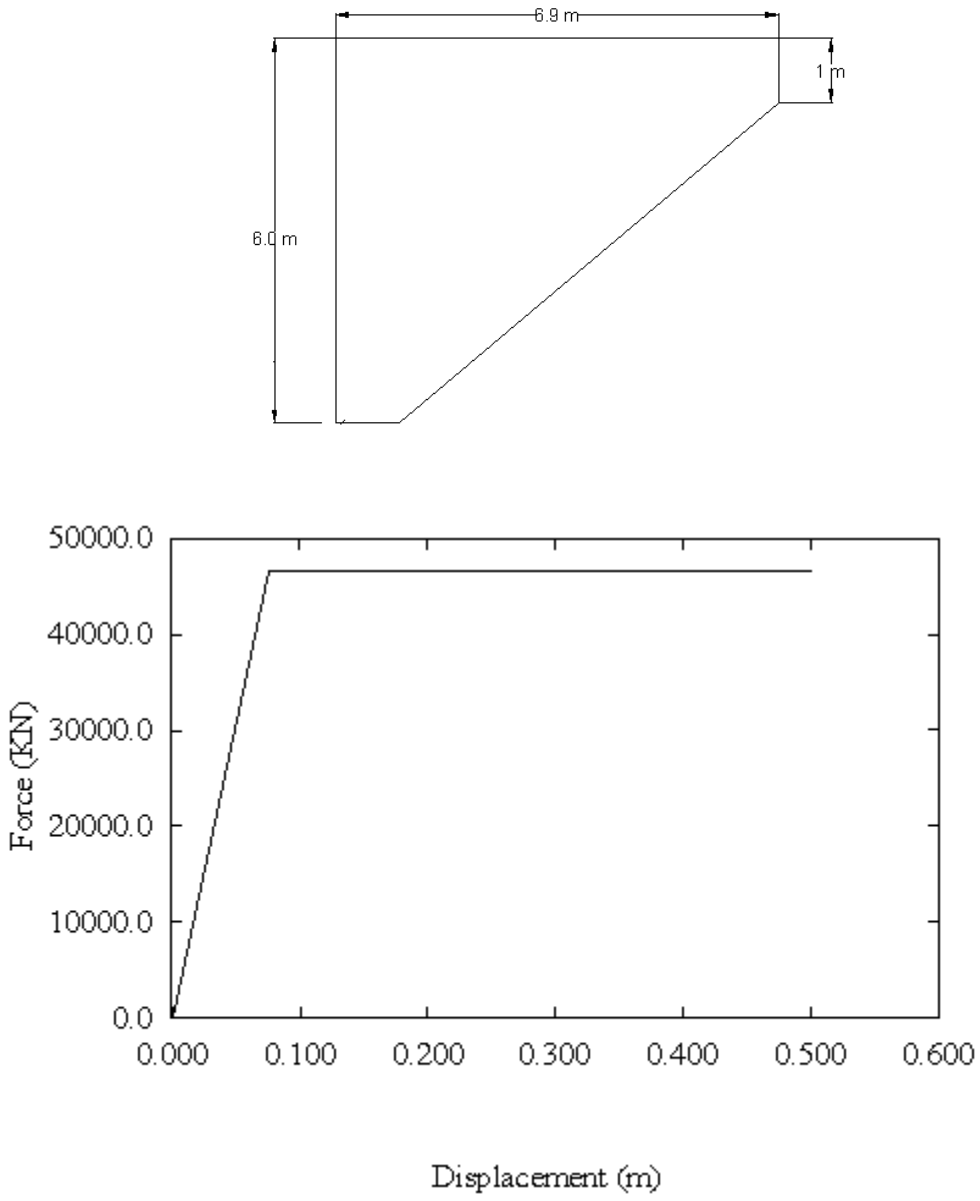

Figure 12: Wingwall Dimensions and Force-displacement response of wing-wall

5.3. Shear Key model

A shear key is included in the abutment in the transverse direction to provide additional transverse stiffness to assess performance of bridge under the suite of time histories. Shear keys form an integral part of bridges with seat type abutments to facilitate the transfer of shear force between the superstructure and the abutment in the transverse direction. They play a crucial role in restraining the structure for transverse movement. In the present study, shear keys are designed to resist 120% of the bent shear capacity. These follow the recommendations of Ramanathan (2012). The authors in their study choose this model based on research by Megally *et al*. (2002) based on a series of experiments on external shear keys in bridge abutments. They discovered that the shear keys undergo a maximum displacement of 3.5 in before their capacity reduces to zero. The force displacement curve is developed based on these recommendations of and can be seen in Figure 13.

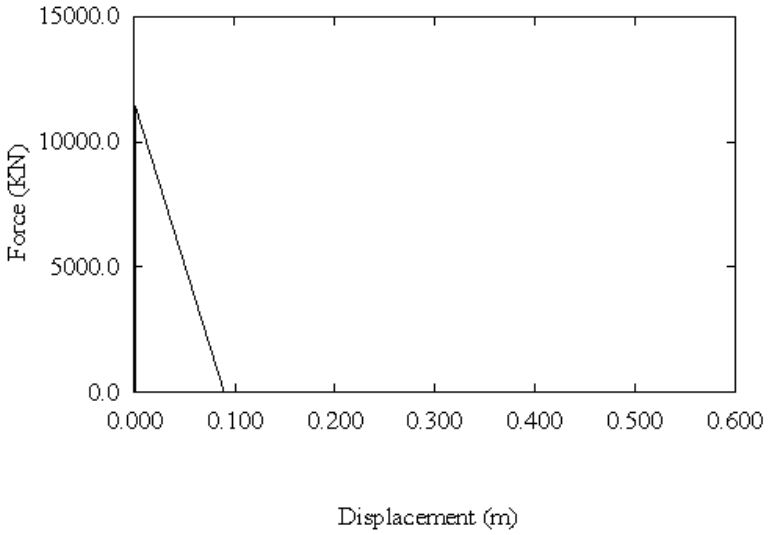

Figure 13: Force-displacement response of shear key

5.4 System Resilience

The system resilience for the as-built bridge and the bridge post-retrofit for different methods are determined. Difference in resilience obtained indicates effectiveness of the method of retrofit used. The different values of resilience are tabulated in Table 14.

The resilience for the as-built structure was determined to 57.47%. From Table 9, it is observed that there is no change in the resilience of the structure when the bridge structure is modeled with an abutment and a shear key on the east end. The resilience of the structure is greatly improved by reinforcing the columns with a steel jacket. This is expected as the structure in majority of the cases fails by shear of the piers

in the transverse direction because of lack of transverse reinforcement. As this issue is addressed using steel jackets, no failure is observed and hence the resilience of the structure is greatly enhanced.

Table 14: Values of Resilience obtained for different retrofits

Steel Jacket – Ohno eqn.	Steel Jacket – FHWA Manual	Abutment Model	Shear Key model
99.76%	99.97%	57.47%	57.47%

On a general note, for other cases of bridges which would experience failure in different modes; while developing the fragility curves, the governing modes should be chosen in such a manner so as to encompass all possibilities of failure. In these cases, other modes of retrofit might prove to be more effective and measuring resilience would show that an enhanced value as opposed to the un-retrofitted structure. For example, drift is expected to be a governing mode in some bridges. Threshold limits are to be developed for drift ratios based on existing codes and manuals and fragility curves are to be developed based on the governing mode of failure before proceeding to evaluation of seismic resilience.

Chapter 6 Sensitivity Study

A sensitivity study is performed to analyze the impact of various uncertain parameters such as recovery time, control time, indirect to direct loss cost ratio and fragility parameters (median values) on the resilience of the unretrofitted bridge. For this study, each parameter is varied individually while keeping all other parameters at their respective mean values. The scatterness of these uncertain parameters is described next.

6.1. Recovery time

The as-built bridge has shear failure. Consequently, a mean recovery time of 75 days is used to calculate the mean resilience of the bridge. To observe the sensitivity of resilience to recovery time, it is varied with a standard deviation of 42 days (HAZUS 1999). Thus, resilience of the as-built is calculated for mean ± standard deviation of the recovery time.

6.2. Control time

The control time T_{LC} is decided by engineers, in general. It depends on the time window of interest, and thus it can be bigger or smaller than the recovery time. The resilience of the as-built bridge is calculated for mean ± standard deviation of the control time to

calculate its effect on bridge resilience. The mean value of control time is taken as 85 days, whereas the standard deviation is considered to be 40 days.

6.3. Indirect to Direct Loss Cost Ratio

The indirect to direct loss ratio may lie between 5 and 20 (Denneman 2009). For this study, a value of 13 is taken as a mean value of this ratio. To cover the possible range of this ratio in the sensitivity study, a standard deviation of 8 is taken here.

6.4. Fragility Parameters

Fragility parameters of the bridge may vary due to the variability of various structural parameters. In the absence of any parametric study with structural parameters, variability (or uncertainty) of fragility curves can be represented in the form of 90% confidence intervals (between 5% and 95% confidence levels) of these curves. In this study, fragility parameters for 5% and 95% confidence levels are estimated following the procedure described in Banerjee and Shinozuka (2008) and Banerjee et al. (2009) and given in Table 15. Resilience of the bridge is estimated for fragility curves with 5% and 95% confidence bands.

Table 15: Fragility parameters for 5% and 95% confidence intervals

Damage State	Median (5% confidence interval)	Median (95% confidence interval)
Minor	0.101	0.13
Moderate	0.197	0.234
Major	0.356	0.407
Collapse	0.389	0.441

6. 5. Results from Sensitivity Analysis

The results of the sensitivity study for all these parameters are tabulated in Table 15. Figure 14 shows a tornado diagram which accurately summarizes the results of the sensitivity study. As the figure elaborates, the resilience is more sensitive to recovery time and control time as opposed to fragility parameters and the indirect to direct loss cost ratio. Results of FOSM (First Order Second Moment) reliability analysis are depicted in Figure 15. It shows the relative variance contribution of different sensitivity parameters and further support the observation observed in tornado diagram.

Table 16: Resilience as a percentage value for different sensitivity parameters

Sensitive Parameter	Mean – SD	Mean	Mean + SD
Recovery time	81.36%	57.47%	40.43%
Control time	32.80%	57.47%	71.20%
Indirect to Direct Loss Cost Ratio	59.14%	57.47%	56.76%
Fragility parameters	57.43%	57.47%	57.56%

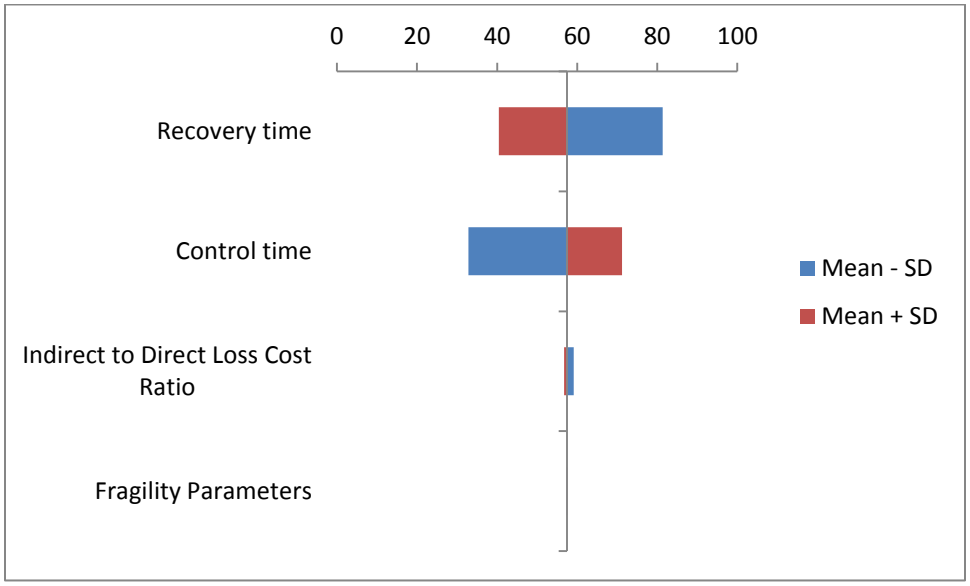

Figure 14: Tornado-Diagram to depict Sensitivity Study

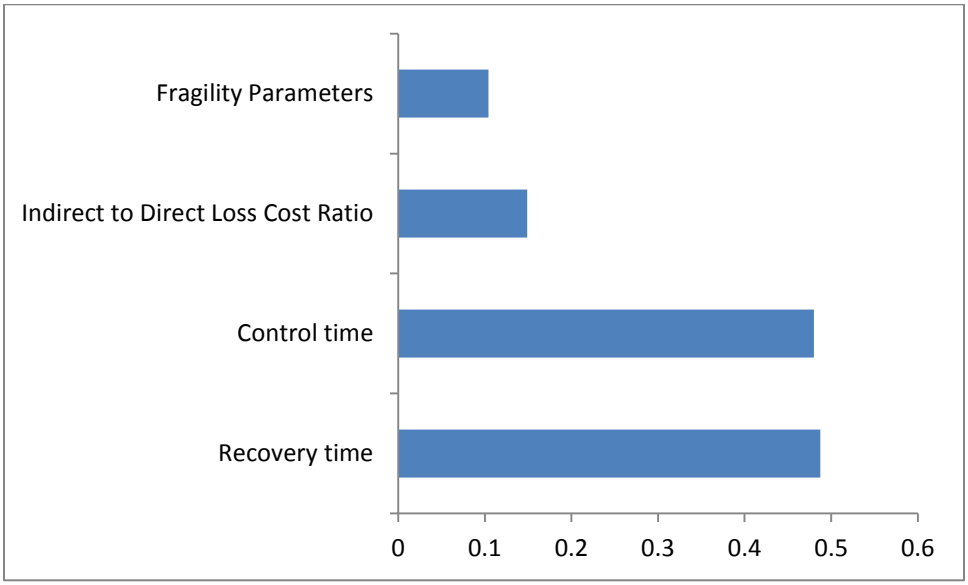

Figure 15: Relative variance contribution from FOSM analysis

Chapter 7 Cost-Benefit Analysis

The original bridge failed during the 1994 Northridge earthquake. Results from this study shows that this failure and associated losses could have been avoided if the bridge piers were retrofitted with steel jackets prior to the Northridge event. In this relation, it is also important to justify the cost associated with seismic retrofitting. Therefore, the cost effectiveness of applied retrofit strategy needs to be judged by calculating the total dollar amount that can be avoided by avoiding any major damage of the bridge under regional future earthquakes. This chapter focuses on cost-benefit analysis of bridge seismic retrofit.

7.1. Cost of Retrofit

The cost of retrofitting Piers 6 to 8 using steel jackets is determined using the Contract Cost Database of the Caltrans website. Historic bid data for Caltrans construction cost data is obtained from the website. A study of history of contract bids for steel jackets revealed that the cost of such a type of retrofit was based on the weight (lb) of concrete of the element that is to be jacketed. The cost is realized as $2/lb. Extending the same to this research based on the weight of concrete of Piers 6 to 8 which are to be retrofitted, the cost of retrofit amounts to $168,800.

7.2. Benefit

7.2.1 Annual Benefit

Prior to any earthquake, Post seismic retrofitting of bridges, losses arising from indirect costs and repair/restoration costs will be reduced significantly. This reduction in loss is the benefit from the seismic retrofit, and is expressed in Eq. (24) as the cost avoided from the indirect costs and repair/restoration cost. Hence, cost avoided from system restoration is estimated as the difference in bridge restoration cost (CRPm) evaluated in cases 1 and 2, where case 1 and 2 represent the bridge before and after retrofit respectively. Similarly, the difference in the system indirect cost estimated is defined as the "system indirect cost avoided". Thus expected annual benefit from bridge retrofit is computed by adding the total cost avoided from the bridge restoration and the indirect cost.

This expected benefit also is dependent on the annual probability of occurrence of the earthquake under consideration. The current research, therefore, uses the following equation (Chang *et al*. 2000, Zhou *et al*. 2009) to obtain the expected annual benefit under *M* scenario earthquakes that may occur in the region of interest.

$$\overline{B} = \sum_{m=1}^{M} [(C_{sm}^{0} - C_{sm}^{R}) + (C_{RPm}^{0} - C_{RPm}^{R})]\overline{p}_{m} \tag{24}$$

where $\overline{B}$ is the expected annual benefit from the bridge retrofit. The parameters C_{sm}^{0} and C_{RPm}^{0} represent system indirect costs and system restoration cost, respectively, under a scenario event *m* when the bridges are not retrofitted and C_{sm}^{R} and C_{RPm}^{R} represent the same when bridges are retrofitted.

The area of Los Angeles has several active seismic faults that are capable in producing hundreds of earthquakes in future. For seismic risk assessment, Chang *et al*. (2000) performed probabilistic seismic hazard analysis and developed a set of 47 scenario earthquakes that approximately represent the seismic hazard of the Los Angeles region. These 47 scenario earthquakes are also used here to perform the cost benefit analysis. The details of these earthquakes are given in Table 16. To predict possible damage of the test-bed bridge (before and after retrofitting with steel jacket) due to these scenario events, intensities of all these events at the bridge site is estimated using the base model of attenuation relation given by Abrahamson and Silva (2008). For each scenario event, distance between seismic source and the test bridge site, PGA at bridge site and failure probabilities of the bridge at various damage states are given in Appendix. Calculated failure probabilities are then used to compute the total cost (direct and indirect) before and after applying the steel jacket. The difference in cost is the benefit from seismic retrofit.

Table 17: Probabilistic Scenario Earthquake Set

Event No.	Scenario EQ	Type	Moment Magnitude	Annual PB	Lat.	Long.
1	Elysian Park	MCE	7.1	0.000728	34.165	-117.833
2	Malibu Coast	MCE	7.3	0.000068	34.007	-118.615
3	Newport-Inglewood(N.)	MCE	7	0.000495	33.975	-118.359
4	Newport-Inglewood(S.)	MCE	7	0.000495	33.66	-117.997
5	Palos Verdes	MCE	7.2	0.00154	33.618	-118.17
6	Raymond	MCE	6.7	0.00065	34.127	-118.12
7	San Andreas	MCE	8	0.00485	34.278	-117.477
8	San Jacinto	MCE	7.5	0.0008	33.882	-117.087
9	Santa Susana	MCE	6.9	0.004362	34.318	-118.599
10	Sierra Madre	MCE	7.4	0.00208	34.143	-117.936
11	Simi Santa Rosa	MCE	7.5	0.000214	34.282	-118.822
12	Verdugo	MCE	6.8	0.00062	34.184	-118.273
13	Whittier	MCE	7.5	0.000312	33.643	-117.348
14	Malibu Coast	U/D	6	0.0003	34.1395	-118.0422
15	Malibu Coast	U/D	6	0.0005	34.1161	-118.1578
16	Malibu Coast	U/D	6	0.0003	34.0944	-118.3717
17	Newport-Inglewood	U/D	6	0.001	33.8961	-118.2691
18	Newport-Inglewood	U/D	6	0.001	34.0079	-118.3739
19	Newport-Inglewood	U/D	6	0.001	33.8168	-118.1971
20	Newport-Inglewood	U/D	6	0.001	33.7369	-118.0793
21	Newport-Inglewood	U/D	6	0.001	33.6448	-117.9549
22	Palos Verdes	U/D	6	0.0016	33.7782	-118.3149
23	San Andreas	U/D	6	0.02	34.4306	-117.8153
24	San Andreas	U/D	6	0.02	34.6266	-118.3192
25	San Jacinto	U/D	6	0.01	34.2631	-117.499
26	Santa Susana	U/D	6	0.01	34.3279	-118.6072
27	San Fernando	U/D	6	0.005	34.2937	-118.4676
28	Sierra Madre	U/D	6	0.01	34.2559	-118.2538
29	Sierra Madre	U/D	6	0.01	34.1605	-117.92
30	Whittier	U/D	6	0.0015	33.9571	-117.9069
31	Malibu Coast	U/D	6.5	0.00015	34.1431	-118.1218
32	Malibu Coast	U/D	6.5	0.00015	34.1092	-118.0727
33	Malibu Coast	U/D	6.5	0.0001	34.0916	-118.3802

34	Newport-Inglewood	U/D	6.5	0.0005	33.9399	-118.3186
35	Newport-Inglewood	U/D	6.5	0.0005	33.7901	-118.1462
36	Newport-Inglewood	U/D	6.5	0.0005	33.6557	-117.9585
37	San Andreas	U/D	6.5	0.008	34.5936	-118.2052
38	San Andreas	U/D	6.5	0.008	34.4388	-117.8385
39	San Jacinto	U/D	6.5	0.005	34.2301	-117.4543
40	Santa Susana	U/D	6.5	0.0011	34.2966	-118.4232
41	Whittier	U/D	6.5	0.001	33.9242	-117.8406
42	Malibu Coast	U/D	7	0.00005	34.0652	-118.456
43	Malibu Coast	U/D	7	0.00005	34.1232	-118.157
44	San Jacinto	U/D	7	0.0015	34.2372	-117.463
45	San Andreas	U/D	7	0.003	34.5726	-118.1789
46	San Andreas	U/D	7	0.003	34.4032	-117.7315
47	Whittier	U/D	7	0.0005	33.9401	-117.8843

7.2.2. Total Benefit

The normal design service life of a highway bridge is generally taken to be 75 years. Due to retrofitting, this study considers an extended service life (T) of the bridge. For analytical purposes, T is taken to be somewhere between 30 to 60 years.

The total benefit (B) of the seismic retrofit in its present value must consider the discount rates into account, and must be computed by adding all discounted benefits over the service life (T) of the bridge. Hence, B is expressed in the form of a uniform series (Zhou et al. 2010):

$$B = \overline{B}\frac{(1+v)^U - 1}{v(1+v)^U} \tag{25}$$

Where $\overline{B}$ the annual benefit of the seismic retrofit as is obtained from Eq. (24); v is the discount rate; T is the time period under consideration. Assuming a discount rate of 3% and 5%, the total benefit is calculated and presented in the Appendix. These values are further used to calculate the benefit to cost ratio to calculate the cost-effectiveness of seismic retrofit.

7.2.3. Cost-Effectiveness

The cost-effectiveness is measured through the ratio of total benefit (B) to the retrofit cost from Section 7.2.1. The cost-effectiveness for the retrofit method is displayed in Table 18 for T ranging from 30 to 60 years for discount rates of 3% and 5%. Figure 16 shows the variation of the benefit-cost ratio with average bridge remaining service life (T) for two different discount rates.

Table 18: Summary of Cost-Benefit Analysis

Discount rate	Service life (years)	Cost-effectiveness
3%	30	1.82
	40	2.14
	50	2.38
	60	2.56
5%	30	1.42
	40	1.59
	50	1.69
	60	1.75

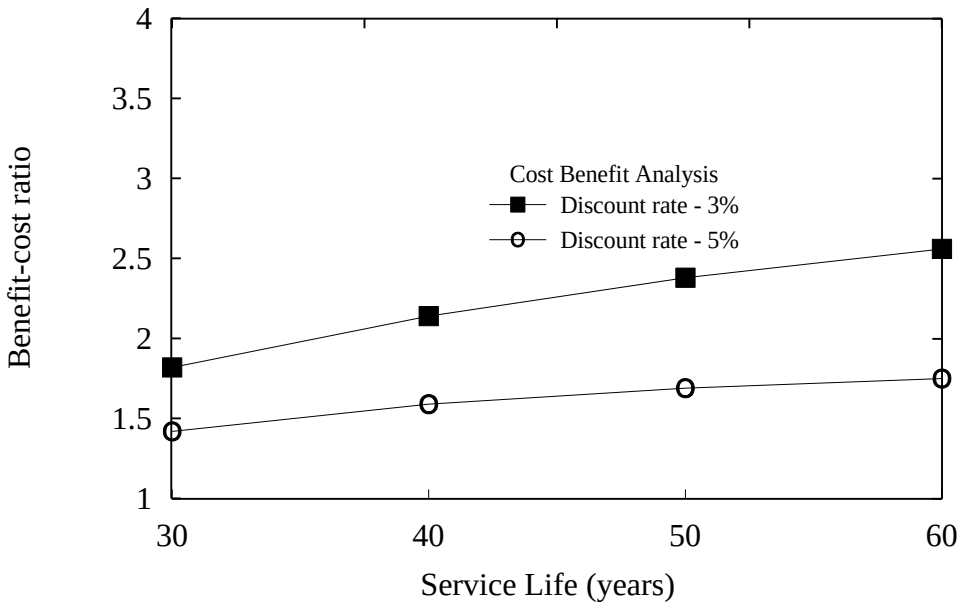

Figure 16: Benefit-cost ratios of seismic retrofitting

The retrofit strategy is cost effective if the benefit to cost ratio is more than 1. As observed from the above figure, the retrofit is cost effective if the normal service life of the bridge is extended beyond 30 years. A higher bridge service life indicates a higher cost-effectiveness of seismic retrofitting. It also shows that retrofitting is more cost-effective for lower discount rate.

Chapter 8 Conclusions and Recommendations

8.1. Conclusions

Seismic performance of a reinforced concrete bridge which experienced severe damage during the 1994 Northridge earthquake is studied here. Ground motion data recorded at the City Hall station in Santa Monica is obtained from the Pacific Earthquake Engineering Centre (PEER) database. This recording station is about 10 km away from the bridge site. Finite element model of the bridge was developed. Bridge piers are modeled using lump plasticity. Bi-linear moment-rotation diagrams are developed to define nonlinear characteristics of plastic hinge regions of bridge piers. Mode shapes and modal time periods for first six fundamental modes of the bridge and shear demand and shear capacity of bridge piers were compared to previous literature for the purpose of model validation. Seismic vulnerability of the bridge is obtained by analyzing the bridge under 60 LA motions, which are considered to represent seismicity of the study region. These motions are applied along the transverse direction of the bridge to capture the bridge response in this direction. Bridge response is measured in terms of rotational ductility at the top of the pier and shear demands. Threshold damage limit states of individual members are obtained using extrapolation methods applied to the moment-rotation diagrams and previous literature. Damage states of the bridge under seismic ground motion are identified by comparing calculated values of rotation ductility with their respective threshold values for these damage states. In case of brittle shear failure, it

is assumed that the bridge would experience the collapse damage state. From bridge damage information, fragility curves are generated which represent the probability of bridge failure at a particular damage state under a certain intensity of ground motion. These curves are a useful tool for seismic risk evaluation of bridges under similar conditions. Probabilities of exceedance for different damage states under the Northridge earthquake ground motion are calculated and incorporated in a loss model to calculate the direct seismic costs incurred. A ratio of indirect to direct costs is assumed to calculate the total loss ratio. A linear recovery model is chosen for this study. The loss ratio coupled with the recovery model is used to obtain the value of seismic resilience of the as-built bridge.

Three different retrofit strategies are applied to the bridge; the above procedure is followed to calculate seismic resilience for each strategy. Effectiveness of retrofit is identified by enhanced value of resilience obtained. It is found that bridge retrofit with steel jacket enhanced seismic resilience of the bridge and the other two retrofit strategies had no effect on it. This study is further extended to measure the variability of uncertain input parameters, mostly in the resilience model, and their sensitivity on resilience. First order second moment (FOSM) reliability is used to evaluate sensitivity of bridge resilience on various parameters such as recovery time, control time, indirect to direct cost ratio and bridge fragility characteristics. A tornado diagram is developed to further support the results from FOSM method. It is found that the seismic resilience is most sensitive to the recovery time and control time and not so sensitive on other parameters. Cost-benefit study is performed assuming a 30 to 60 year enhanced service life of the

jacketed bridge. In this 47 future scenario earthquakes are used to represent the seismicity of the Los Angeles region. Results show that bridge seismic retrofit with steel jacket is cost effective when the service life of the bridge is enhanced beyond 30 years due to retrofit.

8.2. Applications of current study

Several seismically deficient reinforced concrete bridges are still in operation. Most of them were constructed in the second half of the twentieth century prior to the development of any modern seismic design codes. Many of such existing bridges have been either identified for seismic retrofit or already retrofitted in recent past. The test-bed bridge considered in this study represents a bridge from such a bridge class. This bridge was scheduled for seismic retrofitting; however, the Northridge earthquake occurred prior to the schedule retrofit time. Results from this study showed that seismic retrofit not only can improve performance of the bridge, but also effective is in enhancing seismic resilience. In addition, such retrofit strategy is cost effective. Hence, similar retrofit strategy can be applied to bridges that have similar structural attributes (such as number of spans, average span length, number of piers, material properties and reinforcement ratios) to enhance seismic resilience.

The procedure of resilience estimation discussed here is transportable and can easily be applied to other types of bridges and for other hazard scenarios. A general flowchart is presented here to evaluate the seismic resilience of bridges and to determine

effective retrofit strategies. The difference in resilience between the bridge model with retrofit and without retrofit is a measure of the effectiveness of retrofit.

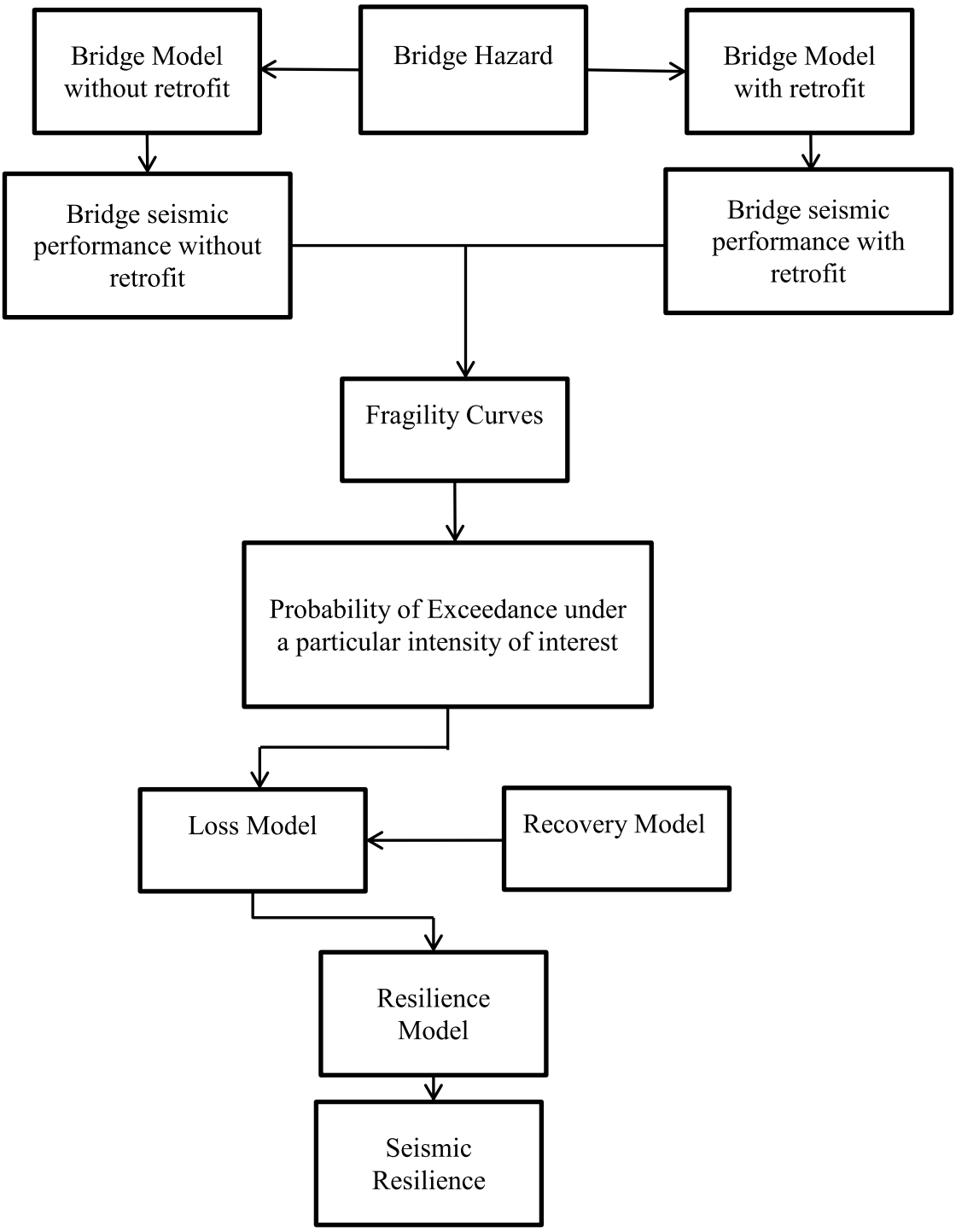

Figure 17: Flow-chart for determining seismic resilience of bridges with and without retrofitting to determine appropriate strategy

8.3. Future Study

Based on the observations made from the present study, future research can explore the following:

- Development of guidelines for adopting cost-effective retrofit strategies for bridges located in seismically active regions.
- Conduct an inter-dependent sensitivity analysis varying more than one parameter at a time. This will result in a better insight into resilience values as parameters in the resilience model are highly uncertain.
- Use of evolutionary algorithms to arrive at cost optimized retrofit strategy to handle seismic hazards with various objectives and constraints as per need. A dominant range of solutions can be obtained through this methodology as a result of optimization of a wide range of objectives.
- The same framework can be extended to other hazard conditions.

References

Abrahamson, N., and Silva, W. (2008). “Summary of the Abrahamson & Silva NGA Ground- Motion Relations.” *Earthquake Spectra*, *24*(1), 67-97.

AIJ, “Standard for Structural Calculation of Reinforced Concrete Structures. Architectural Institute of Japan, 1999.

Alipour, A., Shafei, B., Shinozuka, M. (2010). “Performance Evaluation of Deteriorating Highway Bridges Located in High Seismic Areas.” *Journal of Bridge Engineering* ,2010.

Amdal, J. R., and Swigart, S.L. (2010). "Resilient Transportation Systems in a Post-Disaster Environment: A Case Study of Opportunities Realized and Missed in the Greater New Orleans Region." *UNOTI Publications*: Paper 5.

Arcidiacono, V., Cimellaro, G. P., Reinhorn, A. M., and Bruneau, M. (2012) "Community Resilience Evaluation including interdependencies." *15th World Conference on Earthquake Engineering (15WCEE)*, Lisbon, Portugal, September 24-28th, 2012.

Aviram, A.,Mackie, K.R.,Stojadinovic, B. (2008). "Effect of abutment modeling on the seismic response of bridge structures." *Earthquake Engineering &Engineering Vibrations* 7,pp.395-402.

Aviram, A., Mackie, K.R., Stojadinovic, B. (2008). "Guidelines for Nonlinear Analysis of Bridge Structures in California." *Pacific Earthquake Engineering Research Center Report*, UCB/PEER 2008/03.

Banerjee, S. and Shinozuka, M. (2007). "Nonlinear static procedure for seismic vulnerability assessment of bridges." *Computer-Aided Civil and Infrastructure Engineering* (CACAIE), Computational Structural Engineering, 22(4), 293-305.

Banerjee, S. and Shinozuka, M. 2008a. "Mechanistic quantification of RC bridge damage states under earthquake through fragility analysis." *Probabilistic Engineering Mechanics*, 23(1), 12-22.

Banerjee, S. and Shinozuka, M. 2008b. "Experimental verification of bridge seismic damage states quantified by calibrating analytical models with empirical field data" *Journal of Earthquake Engineering and Engineering Vibration*, 7(4), 383-393.

Banerjee, S. and Ganesh Prasad, G. (2012) "Seismic Risk Assessment of Reinforced Concrete Bridges in Flood-Prone Regions" *Structure and Infrastructure Engineering*.

Bentley Structures, STAADPro Section Designer, Yorba Linda, CA, 2011.

Broderick, B.M. and Elnashai, A.S (1994). "Analysis of the failure of Interstate 10 Freeway ramp during the Northridge earthquake of 17 January 1994." *Earthquake Engineering and Structural Dynamics*, Vol. 24, 189-208.

Bruneau, M., Chang, S., Eguchi, R., Lee, G., O'Rourke, T., Reinhorn, A., Shinozuka, M., Tierney, K., Wallace, W. and von Winterfelt, D., (2003). "A Framework to quantitatively assess and enhance the Seismic Resilience of Communities." *EERI Spectra Journal*, Vol.19, No.4, pp.733-752.

Bruneau, M., and Reinhorn, A. (2007). "Exploring the concept of seismic resilience for acute care facilities." *Earthquake Spectra* ; 23(1) : 41-63

Bozorgzadeh, A.,Megally, S.H.,Ashford, S.,Restrepo, J.I. (2007). "Seismic Response of Sacrifical Exterior Shear Keys in Bridge Abutments." Structural Systems Research Project, Report No. SSRP-04/14.

Cagnan, Z., Davidson, R.A., Guikema, S.D. (2005). "Post-Earthquake Restoration Planning for Los Angeles Electric Power." *Earthquake Spectra* : August 2006, Vol. 22, No. 3, pp. 589-608.

Caltrans (1997). *Seismic Design References*. State of California Department of Transportation Division of Structures.

Caltrans (2004). Seismic Design Criteria, California Department of Transportation, Division of Structures, Sacremento, CA.

Caltrans (2011). Seismic Retrofit Program, http://www.dot.ca.gov/hq/paffairs/about/retrofit.htm, as visited on February 14, 2011.

Chai, Y. H., Priestley, M. N., and Seible, F. (1991). "Seismic Retrofit of Circular Bridge Columns for Enhanced Flexural Performance." *ACI Structural Journal (American Concrete Institute)*, 88(5), 572–584.

Chang, S. and Chamberlin, C. (2004). "Assessing the Role of Lifeline Systems and Community Disaster Resilience." *MCEER Research Progress and Accomplishments*, 2003-04. Buffalo, NY.

Chang, S.E. and Nojima, N. (2001). "Measuring Post-Disaster Transportation System Performance: The 1995 Kobe Earthquake in Comparative Perspective." *Transportation Research Part A: Policy and Practice*, 35(6):475-494.

Chang, S.E., and Shinozuka, M., (2004). "Measuring Improvements in the Disaster Resilience of Communities." *Earthquake Spectra* ; 20(3) :pp.739-55.

Choi, E. (2002). "Seismic Analysis and Retrofit of Mid-America Bridges.," Georgia Institute of Technology, in partial requirement for the requirement for Doctor of Philosophy.

Computer and Structures, Inc. (1995).,SAP2000 (Structural Analysis Program),Berkeley, CA, Version 15.0.

Computer and Structures, Inc. (1995).,SAP2000 Non-linear Users Manual., V.8, Berkeley, CA.

Cofer, W.F., Mclean D.I., Zhang, Y. (1997). "Analytical Evaluation of Retrofit Strategies for Multi-Column Bridges." *Technical Report for Washington State Transportation Centre (TRAC*), Washington State University, Pullman, Washington

Cimellaro, G.P. (2008). "Improving Seismic Resilience of Structural Systems Through Integrated Design of Smart Structures." PhD Dissertation, State University of New York at Buffalo, NY.

Cimerallo, G.P., Reinhorn, A.M., and Bruneau, M. (2010). "Framework for analytical quantification of disaster resilience." *Engineering Structures* 32: pp.3639–3649

Dennemann, L.K. (2009). "Life-Cycle Cost Benefit (LCC-B) Analysis for Bridge Seismic Retrofits." MS Thesis, Rice University, TX.

Frangopol, D.M., and Bocchini, P., (2011). "Resilience as Optimization Criterion for the Rehabilitation of Bridges belonging to a Transportation Network Subject to Earthquake." In Proceedings of the *2011 Structure Congress* ,ASCE: pp. 2044-2055.

Ganesh Prasad, G. and Banerjee, S**.** (2013) "The Impact of Flood-Induced Scour on Seismic Fragility Characteristics of Bridges." *Journal of Earthquake Engineering*, Accepted for publication.

HAZUS 1999. Earthquake Loss Estimation Methodology, *Technical Manual SR2*, Federal Emergency Management Agency through agreements with National Institute of Building Science, Washington, D.C.

Kelly, J. M. (1997). *Earthquake-Resistant Design with Rubber*. Springer, London, second edition.

FHWA, Seismic Retrofitting Manual for Highway Structures: Part 1 – Bridges. (2006), Publication No. FHWA-HRT-06-032, January 2006.

Lee, D.H. and Elnashai, A.S. (2002). “Inelastic seismic analysis of RC Bridge Piers including flexure-shear interaction.” *Structural Engineering and Mechanics*,Vol. 12 ,No.3 pp:241-260.

Mackie, K.R., Wong, J-M., and Stojadinovic, B. (2010). "Post-earthquake bridge repair cost and repair time estimation methodology." *Earthquake Engineering and Structural Dynamics,* 39(3): 281-301.

Maroney, B.H. and Chai, Y.H. (1994). “Seismic Design and retrofitting of reinforced concrete bridges.”*Proceedings of 2nd International Workshop, Earthquake Commission of New Zealand*, Queenstown,New Zealand.

Miles, S.B. and Chang, S.E. (2004). “Foundations for modeling community recovery from earthquake disasters.” *13th World Conference on Earthquake Engineering*, Vancouver, B.C., Canada, August 1-6, 2004, Paper No.567.

Maroney, B., Kutter, B., Romstad, K., Chai, Y. H., and Vanderbilt, E. (1995). “Interpretation of Large Scale Bridge Abutment Test Results.” *Proceedings of 3rd Annual Seismic Research Workshop,* Sacramento, CA. Caltrans.

Megally, S. H., Silva, P. F., Seible, F. (2002). "*Seismic Response of Sacrificial Shear Keys in Bridge Abutments",* Structural Systems Research Project SSRP-2001/24, University of California, San Diego, La Jolla, CA.

Na, U.J.,Chaudhuri, S.R. and Shinozuka, M. (2008). "Probabilistic assessment for seismic performance of port structures." *Soil Dynamics and Earthquake Engineering* 28,pp.147-158.

Nielson, G. B. (2005). "Analytical Fragility Curves for Highway Bridges in Moderate Seismic Zones." Georgia Institute of Technology, in partial requirement for the requirement for Doctor of Philosophy.

Nielson, B.G and DesRoches, R. (2006). "Influence of modeling assumptions on the seismic response of multi-span simply supported steel girder bridges in moderate seismic zones." *Engineering Structures* 28 (2006) 1083–1092.

Nielson, B.G. and DesRoches, R. (2007). "Seismic Performance Assessment of Simply Supported and Continuous Multispan Concrete Girder Highway Bridges." *Journal of Bridge Engineering*,Vol. 12,No. 5 ,September/October 2007, pp:611-620.

Nielson, B.G. and DesRoches, R. 2007. "Analytical Seismic Fragility Curves for Typical Bridges in the Central and Southeastern United States." *Earthquake Spectra*, Volume 23, No. 3, pp: 615–633, August 2007, Earthquake Engineering Research Institute.

Padgett, J.E. (2007). “Seismic Vulnerability Assessment of retrofitted Bridges using Probabilistic Methods.” Georgia Institute of Technology, in partial requirement for the requirement for Doctor of Philosophy.

Padgett, J.E, Dennemann, K., Ghosh, J. (2010). “Risk-based seismic life-cycle cost-benefit (LCC-B) analysis for bridge retrofit assessment” *Structural Safety* 32 pp.165–173.

Paton, D., and Johnston, D. (2006). "Disaster resilience an integrated approach." *Charles C Thomas publisher LTD.*, Cap. 4," lifelines and urban resilience".

Penzien, J., Seible, F., Bolt, B.A., Idriss, I.M., Nicoletti, J.P., Preece, R.F. and Roberts, E.R., (2003). ”The race to Seismic Safety.” Report submitted to Director, California Department of Transportation, December 2003.

Priestley, M.J.N., Seible, F., Calvi, G.M. (1996), Seismic Design and Retrofit of Bridges, John Wiley & Sons, Inc., New York, N.Y.

Ramanathan, K.N. (2012). “Next generation Seismic Fragility Curves for California Bridges incorporating the evolution in seismic design philosophy.” Georgia Institute of Technology ,in partial requirement for the requirement for Doctor of Philosophy.

Rose, A., and Liao, S.E., (2005). "Modeling Regional Economic Resiliency to Earthquakes: A Computable General Equilibrium Analysis of Water Service Disruptions." *Journal of Regional Science* 45: pp.75-112.

Sakino, K. and Sun, Y. (2000). "Steel Jacketing for improvement of column strength and ductility"*12th World Conference on Earthquake Engineering*, Auckland, January 30 – February 4,New Zealand.

Shirole, A. M. and Holt, R. C. (1991). "Planning for a compressive bridge safety assurance program." *Transp. Res. Rec. No. 1290*, Transportation Research Board, Washington D.C., pp. 39-51.

Shinozuka, M., Chang, S. E., Cheng, T.C., Feng, M., O'Rourke, T. D., Saadeghvaziri., M. A., Dong, X., Jin, X., Wang, Y. and Shi, P. 2004. "Resilience of Integrated Power and Water Systems." *MCEER Research Progress and Accomplishments*, 2003-2004, pp. 65-86. Buffalo, NY.

Todd, D., Carino, N., Chung, R.M., Lew, H.S., Taylor, A.W., Walton, W.D., Cooper, J.D. and Nimis, R. (1994). "1994 Northridge Earthquake : Performance of Structures, Lifelines, and Fire Protection Systems." *National Institute of Standards and Technology*, Special Publication 862.

U.S. Department of Transportation, (2002). John A. Volpe National Transportation Systems Center, "Effects of Catastrophic Events on Transportation System Management and Operations, Northridge Earthquake – January 17,1994.".

Warn, G. P. and Ryan, K.L.(2012). "A review of Seismic Isolation for Buildings : Historical Development and Research Needs." *Buildings ISSN 2075-5309*.

Wright, T., DesRoches, R., and Padgett, J.E. (2011). "Bridge Seismic Retrofitting Practices in the Central and Southeastern United States." *Journal of Bridge Engineering*, 16(1): pp. 82-92.

WSDOT(2011). Washington State's Bridge Seismic Retrofit Program, http://www.wsdot.wa.gov/eesc/bridge/preservation/pdf%5CBrgSeismicPaper.pdf, as visited on February 14, 2011.

Zhou, Y., Banerjee, S., and Shinozuka, M. 2010. "Socio-economic effect of seismic retrofit of bridges for highway transportation networks: A pilot study." *Structure and Infrastructure Engineering*, 6 (1–2), 145–157

Appendix: Cost-Benefit Analysis tables

Table 19: Post-earthquake Annual Benefits post retrofits for Discount rate = 3%, T=30 to 60 years

								Discount Rate = 3			
Event	**Scenario EQ**	**Rrup (km)**	**PGA**	**Probability of exceedance (UR) Probability of exceedance(R)**							
No.				**Minor**	**Moderate**	**Major**	**Collapse**	**Annual Benefit (T=30)**	**Annual Benefit (T=40)**	**Annual Benefit (T=50)**	**Annual Benefit (T=60)**
1	Elysian Park	52.89	0.056	7.5E-02(UR) 2.06E-10(R)	3.7E-03 (UR) 4.83E-32(R)	6.16E-05(UR) 4.83E-32(R)	3.13E-05 (UR) 4.83E-32(R)	756.07	891.47	992.54	1067.76
2	Malibu Coast	22.53	0.129	5.91E-01(UR) 2.32E-06(R)	1.6E-01 (UR) 4.38E-24(R)	0.015 (UR) 4.38E-24 (R)	0.009 (UR) 4.38E-24(R)	1010.39	1191.34	1326.40	1426.92
3	Newport-Inglewood(N.)	2.8	0.414	9.95E-01 (UR) 2.06E-10(R)	9.07E-01(UR) 5.7E-15(R)	0.564(UR) 5.7E-15(R)	0.499(UR) 5.7E-15(R)	80645.07	95087.12	105867.23	113890.59
4	Newport-Inglewood(S.)	37.62	0.070	1.6E-01 (UR) 3.25E-09(R)	1.30E-02(UR) 8.5E-30 (R)	3.45E-04(UR) 8.5E-30(R)	1.88E-04(UR) 8.5E-30(R)	1182.74	1394.54	1552.64	1670.31
5	Palos Verdes	46.17	0.068	1.47E-01(UR) 2.30E-09(R)	1.1E-02(UR) 4.39E-30(R)	2.79E-04(UR) 4.39E-30(R)	1.51E-04(UR) 4.39E-30(R)	3320.42	3915.04	4358.90	4689.24
6	Raymond	27.18	0.077	2.11E-01(UR) 9.97E-09(R)	2.1E-02(UR) 7.28E-29(R)	6.81E-04(UR) 7.28E-29(R)	3.82E-04(UR) 7.28E-29(R)	2148.91	2533.74	2821.00	3034.79

7	San Andreas	87.95	0.078	2.19E-01(UR) 8.57E-09(R)	2.2E-02(UR) 5.44E-29(R)	7.44E-04(UR) 5.44E-29(R)	4.19E-04(UR) 5.44E-29(R)	16730.52	19726.65	21963.08	23627.59
8	San Jacinto	119.1	0.040	1.7E-02 (UR) 2.22E-12 (R)	4E-04(UR) 1.37E-35(R)	3.2E-06(UR) 1.37E-35(R)	1.47E-06(UR) 1.37E-35(R)	176.88	208.55	232.19	249.79
9	Santa Susana	41.3	0.060	9.7E-02 (UR) 4.94E-10 (R)	5.5E-03(UR) 2.44E-31(R)	1.07E-04(UR) 2.44E-31(R)	5.57E-05(UR) 2.44E-31(R)	5897.58	6953.72	7742.07	8328.82
10	Sierra Madre	43.16	0.082	2.49E-01(UR) 2.05E-08 (R)	2.76E-02(UR) 2.95E-28(R)	1.04E-04(UR) 2.95E-28(R)	5.98E-04(UR) 2.95E-28(R)	8434.58	9945.06	11072.54	11911.69
11	Simi Santa Rosa	52.16	0.076	2.04E-01(UR) 8.57E-09 (R)	1.93E-02(UR) 5.44E-29(R)	6.21E-04(UR) 5.44E-29(R)	3.47E-04(UR) 5.44E-29(R)	677.44	798.75	889.31	956.71
12	Verdugo	22.54	0.099	3.82E-01 (UR) 1.61E-07 (R)	6.18E-02(UR) 1.77E-26(R)	3.45E-03(UR) 1.77E-26(R)	2.09E-03(UR) 1.77E-26(R)	4450.39	5247.38	5842.28	6285.04
13	Whittier	102.4	0.045	3E-02 (UR) 1.14E-11 (R)	9.1E-04(UR) 2.51E-34(R)	9.47E-06(UR) 2.51E-34(R)	4.5E-06(UR) 2.51E-34(R)	122.85	144.85	161.27	173.49
14	Malibu Coast	34.12	0.034	7E-03 (UR) 2.12E-13 (R)	1.18E-04(UR) 2.25E-37(R)	6.57E-07(UR) 2.25E-37(R)	2.86E-07(UR) 2.25E-37(R)	27.77	32.74	36.46	39.22
15	Malibu Coast	23.58	0.052	5.6E02(UR) 7.88E-11 (R)	2.34-03(UR) 8.3E-33(R)	3.33E-05(UR)8.3E-33(R)	1.66E05(UR) 8.3E-33(R)	377.04	444.56	494.96	532.47

16	Malibu Coast	10.7	0.121	5.41E-01(UR) 1.25E-06 (R)	0.127(UR) 1.19E-24(R)	1.08E-02(UR) 1.19E-24(R)	6.9E-03(UR) 1.19E-24(R)	3760.86	4434.37	4937.09	5311.26
17	Newport-Inglewood	14.73	0.087	2.88E-01(UR) 3.97E-08 (R)	3.61E-02(UR) 1.08E-27(R)	1.54E-03(UR) 1.08E-27(R)	9E-04(UR) 1.08E-27(R)	4881.64	5755.86	6408.40	6894.08
18	Newport-Inglewood	1.118	0.352	9.87E-01(UR) 5E-03(R)	8.41E-01(UR) 4.24E-16(R)	4.35E-01(UR) 4.24E-16(R)	3.72E-01(UR) 4.24E-16(R)	131167.22	154656.86	172190.43	185240.23
19	Newport-Inglewood	25.77	0.047	3.7E-02(UR) 2.06E-11 (R)	1.22E-03(UR) 7.25E-34(R)	1.39E-05(UR) 7.25E-34(R)	6.72E-06(UR) 7.25E-34(R)	481.91	568.21	632.63	680.57
20	Newport-Inglewood	39.62	0.029	3E-03(UR) 4.83E-17 (R)	3.23E-05(UR) 3.64E-39(R)	1.26E-07(UR) 3.64E-39(R)	5.23E-08(UR) 3.64E-39(R)	36.19	42.67	47.51	51.11
21	Newport-Inglewood	54.95	0.020	2.34E-04(UR) 4.83E-17 (R)	1.08E-06(UR) 1.62E-43(R)	1.83E-09(UR) 1.62E-43(R)	6.73E-10(UR) 1.62E-43(R)	2.84	3.35	3.73	4.01
22	Palos Verdes	25	0.048	4E-02 (UR) 2.73E-11 (R)	1.41E-03(UR) 1.21E-33(R)	1.68E-05(UR) 1.21E-33(R)	8.13E-06(UR) 1.21E-33(R)	848.54	1000.50	1113.92	1198.34
23	San Andreas	70.17	0.015	2.31E-05(UR) 3.22E-19 (R)	5.36E-08(UR) 4.74E-47(R)	4.77E-11(UR) 4.74E-47(R)	1.6E-11(UR) 4.74E-47(R)	5.58	6.58	7.32	7.88
24	San Andreas	70.04	0.015	2.31E-05(UR) 3.22E-19 (R)	5.36E-08(UR) 4.74E-47(R)	4.77E-11(UR) 4.74E-47(R)	1.6E-11(UR) 4.74E-47(R)	5.58	6.58	7.32	7.88

25	San Jacinto	85.48	0.012	3.07E-06(UR) 5.27E-21 (R)	4.20E-09(UR) 6.86E-50(R)	2.25E-12(UR) 6.86E-50(R)	7.03E-13(UR) 6.86E-50(R)	0.37	0.44	0.49	0.53
26	Santa Susana	42.62	0.026	1E-03(UR) 3.51E-15 (R)	1.26E-05(UR) 2.03E-40(R)	3.85E-08(UR) 2.03E-40(R)	1.54E-08(UR) 2.03E-40(R)	180.38	212.68	236.80	254.74
27	San Fernando	34.05	0.034	7E-03(UR) 2.12E-13 (R)	1.18E-04(UR) 2.25E-37(R)	6.57E-07(UR) 2.25E-37(R)	2.86E-07(UR) 2.25E-37(R)	462.84	545.73	607.60	653.65
28	Sierra Madre	30.61	0.038	1.7E-02(UR) 1.07E-12 (R)	2.75E-04(UR) 3.78E-36(R)	1.96E-06(UR) 3.78E-36(R)	8.85E-07(UR) 3.78E-36(R)	1695.73	1999.41	2226.08	2394.79
29	Sierra Madre	45.27	0.025	1.3E-02 (UR) 1.88E-15 (R)	8.84E-06(UR) 7.1E-41(R)	2.48E-08(UR) 7.1E-41(R)	9.8E-09(UR) 7.1E-41(R)	139.02	163.91	182.49	196.32
30	Whittier	43.01	0.026	1E-03(UR)3.51E-15 (R)	1.3E-05(UR)2.03E-40(R)	3.85E-08(UR)2.03E-40(R)	1.54E-08(UR)2.03E-40(R)	27.06	31.90	35.52	38.21
31	Malibu Coast	28.01	0.064	1.21E-01 (UR) 1.10E-09 (R)	7.93E-03(UR) 1.09E-30(R)	1.77E-04(UR) 1.09E-30(R)	9.37E-05(UR) 1.09E-30(R)	259.23	305.66	340.31	366.10
32	Malibu Coast	30.08	0.060	9.7E-02(UR) 4.93E-10 (R)	5.52E-03(UR) 2.44E-31(R)	1.07E-04(UR) 2.44E-31(R)	5.57E-05(UR) 2.44E-31(R)	202.81	239.12	266.23	286.41
33	Malibu Coast	10.42	0.165	7.65E-01(UR) 2.17E-05 (R)	3.02E-01(UR) 5.76E-22(R)	4.66E-02(UR) 5.76E-22(R)	3.27E-02(UR) 5.76E-22(R)	2780.02	3277.87	3649.48	3926.07

34	Newport-Inglewood	8.053	0.205	8.76E-01(UR) 1.29E-04 (R)	4.67E-01(UR) 3.48E-20(R)	1.07E-01(UR) 3.48E-20(R)	7.96E-22(UR) 3.48E-20(R)	23282.46	27451.92	30564.17	32880.53
35	Newport-Inglewood	31.08	0.058	8.6E-02 (UR) 3.22E-10 (R)	4.54E-03(UR) 1.1E-31(R)	8.18E-05(UR) 1.1E-31(R)	4.21E-05(UR) 1.1E-31(R)	591.67	697.63	776.72	835.58
36	Newport-Inglewood	53.83	0.033	6E-03 (UR) 1.36E-13(R)	9.31E-05(UR) 1.04E-37(R)	4.86E-07(UR) 1.04E-37(R)	2.09E-07(UR) 1.04E-37(R)	39.06	46.06	51.28	55.17
37	San Andreas	67.93	0.026	1E-03 (UR) 3.51E-15 (R)	1.26E-05(UR) 2.03E-40(R)	3.85E-08(UR) 2.03E-40(R)	1.54E-08(UR) 2.03E-40(R)	144.30	170.15	189.44	203.79
38	San Andreas	69.22	0.025	1E-03 (UR) 1.88E-15(R)	8.84E-06(UR) 7.1E-41(R)	2.48E-08(UR) 7.1E-41(R)	9.8E-09(UR) 7.1E-41(R)	111.21	131.13	146.00	157.06
39	San Jacinto	88.25	0.020	2.34E-04(UR) 4.84E-17 (R)	1.08E-06(UR) 1.62E-43(R)	1.83E-09(UR) 1.62E-43(R)	6.73E-10(UR) 1.62E-43(R)	14.20	16.74	18.64	20.05
40	Santa Susana	33.53	0.053	6.1E-02 (UR) 1.01E-10(R)	2.6E-03(UR) 1.31E-32(R)	3.91E-05(UR) 1.31E-32(R)	1.96E-05(UR) 1.31E-32(R)	899.48	1060.56	1180.80	1270.29
41	Whittier	49.55	0.036	1E-02(UR) 4.91E-13 (R)	1.83E-04(UR) 9.64E-37(R)	1.16E-06(UR) 9.64E-37(R)	5.14E-07(UR) 9.64E-37(R)	127.00	149.75	166.73	179.36
42	Malibu Coast	10.82	0.202	8.7E-01(UR) 1.14E-04 (R)	4.55E-01(UR) 2.65E-20(R)	1.01E-01(UR) 2.65E-20(R)	7.54E-02(UR) 2.65E-20(R)	2251.08	2654.21	2955.12	3179.08

43	Malibu Coast	24.11	0.104	4.2E-01(UR) 2.70E-07 (R)	7.47E-02(UR) 5.04E-26(R)	4.64E-03(UR) 5.04E-26(R)	2.85E-03(UR) 5.04E-26(R)	413.24	487.24	542.48	583.59
44	San Jacinto	87.69	0.033	6E-03(UR) 1.36E-13 (R)	9.31E-05(UR) 1.04E-37(R)	4.86E-07(UR) 1.04E-37(R)	2.09E-07(UR) 1.04E-37(R)	117.19	138.18	153.84	165.50
45	San Andreas	66.26	0.042	2.2E-02(UR)4.40E-12 (R)	5.67E-04(UR)4.59E-35(R)	5.05E-06(UR)4.59E-35(R)	2.35E-06(UR)4.59E-35(R)	846.93	998.60	1111.81	1196.07
46	San Andreas	74.02	0.038	1.3E-02 (UR) 1.07E-12 (R)	2.75E-04(UR) 3.78E-36(R)	1.96E-06(UR) 3.78E-36(R)	8.85E-07(UR) 3.78E-36(R)	508.72	599.82	667.82	718.44
47	Whittier	45.35	0.059	9.1E-02 (UR) 3.99E-10(R)	5.01E-03(UR) 1.65E-31(R)	9.38E-05(UR) 1.65E-31(R)	4.85E-05(UR) 1.65E-31(R)	633.04	746.40	831.02	894.00
TOTAL ANNUAL BENEFIT								302876.05	357115.59	397602.08	427735.15
BENEFIT-COST RATIO								1.82	2.14	2.38	2.56

Table 20: Post-earthquake Annual Benefits post retrofits for Discount rate = 5%, T= 30 to 60 years

								Discount Rate =5			
Event No.	**Scenario EQ**	**Rrup (km)**	**PGA**	**Probability of exceedance (UR) Probability of exceedance(R)**				**Annual Benefit (T=30)**	**Annual Benefit (T=40)**	**Annual Benefit (T=50)**	**Annual Benefit (T=60)**
				Minor	**Moderate**	**Major**	**Collapse**				
1	Elysian Park	52.89	0.056	7.5E-02(UR) 2.06E-10(R)	3.7E-03 (UR) 4.83E-32(R)	6.16E-05(UR) 4.83E-32(R)	3.13E-05 (UR) 4.83E-32(R)	592.90	661.56	704.38	730.23
2	Malibu Coast	22.53	0.129	5.91E-01(UR) 2.32E-06(R)	1.6E-01 (UR) 4.38E-24(R)	0.015 (UR) 4.38E-24 (R)	0.009 (UR) 4.38E-24(R)	792.33	884.09	941.31	975.85
3	Newport-Inglewood(N.)	2.8	0.414	9.95E-01 (UR) 2.06E-10(R)	9.07E-01(UR) 5.7E-15(R)	0.564(UR) 5.7E-15(R)	0.499(UR) 5.7E-15(R)	63240.55	70564.44	75131.58	77888.33
4	Newport-Inglewood(S.)	37.62	0.070	1.6E-01 (UR) 3.25E-09(R)	1.30E-02(UR) 8.5E-30 (R)	3.45E-04(UR) 8.5E-30(R)	1.88E-04(UR) 8.5E-30(R)	927.48	1034.89	1101.87	1142.30
5	Palos Verdes	46.17	0.068	1.47E-01(UR) 2.30E-09(R)	1.1E-02(UR) 4.39E-30(R)	2.79E-04(UR) 4.39E-30(R)	1.51E-04(UR) 4.39E-30(R)	2603.82	2905.37	3093.41	3206.91
6	Raymond	27.18	0.077	2.11E-01(UR) 9.97E-09(R)	2.1E-02(UR) 7.28E-29(R)	6.81E-04(UR) 7.28E-29(R)	3.82E-04(UR) 7.28E-29(R)	1685.14	1880.30	2002.00	2075.46
7	San Andreas	87.95	0.078	2.19E-01(UR) 8.57E-09(R)	2.2E-02(UR) 5.44E-29(R)	7.44E-04(UR) 5.44E-29(R)	4.19E-04(UR) 5.44E-29(R)	13119.80	14639.21	15586.70	16158.61

8	San Jacinto	119.1	0.040	1.7E-02 (UR) 2.22E-12 (R)	4E-04(UR) 1.37E-35(R)	3.2E-06(UR) 1.37E-35(R)	1.47E-06(UR) 1.37E-35(R)	138.70	154.77	164.78	170.83
9	Santa Susana	41.3	0.060	9.7E-02 (UR) 4.94E-10 (R)	5.5E-03(UR) 2.44E-31(R)	1.07E-04(UR) 2.44E-31(R)	5.57E-05(UR) 2.44E-31(R)	4624.78	5160.38	5494.38	5695.98
10	Sierra Madre	43.16	0.082	2.49E-01(UR) 2.05E-08 (R)	2.76E-02(UR) 2.95E-28(R)	1.04E-04(UR) 2.95E-28(R)	5.98E-04(UR) 2.95E-28(R)	6614.26	7380.26	7857.93	8146.26
11	Simi Santa Rosa	52.16	0.076	2.04E-01(UR) 8.57E-09 (R)	1.93E-02(UR) 5.44E-29(R)	6.21E-04(UR) 5.44E-29(R)	3.47E-04(UR) 5.44E-29(R)	531.23	592.76	631.12	654.28
12	Verdugo	22.54	0.099	3.82E-01 (UR) 1.61E-07 (R)	6.18E-02(UR) 1.77E-26(R)	3.45E-03(UR) 1.77E-26(R)	2.09E-03(UR) 1.77E-26(R)	3489.93	3894.09	4146.13	4298.26
13	Whittier	102.4	0.045	3E-02 (UR) 1.14E-11 (R)	9.1E-04(UR) 2.51E-34(R)	9.47E-06(UR) 2.51E-34(R)	4.5E-06(UR) 2.51E-34(R)	96.33	107.49	114.45	118.65
14	Malibu Coast	34.12	0.034	7E-03 (UR) 2.12E-13 (R)	1.18E-04(UR) 2.25E-37(R)	6.57E-07(UR) 2.25E-37(R)	2.86E-07(UR) 2.25E-37(R)	21.78	24.30	25.87	26.82
15	Malibu Coast	23.58	0.052	5.6E02(UR) 7.88E-11 (R)	2.34E-03(UR)8.3E-33(R)	3.33E-05(UR)8.3E-33(R)	1.66E-05(UR)8.3E-33(R)	295.67	329.91	351.26	364.15
16	Malibu Coast	10.7	0.121	5.41E-01(UR) 1.25E-06 (R)	0.127(UR) 1.19E-24(R)	1.08E-02(UR) 1.19E-24(R)	6.9E-03(UR) 1.19E-24(R)	2949.21	3290.76	3503.74	3632.30

17	Newport-Inglewood	14.73	0.087	2.88E-01(UR) 3.97E-08 (R)	3.61E-02(UR) 1.08E-27(R)	1.54E-03(UR) 1.08E-27(R)	9E-04(UR) 1.08E-27(R)	3828.11	4271.44	4547.90	4714.77
18	Newport-Inglewood	1.118	0.352	9.87E-01(UR) 5E-03(R)	8.41E-01(UR) 4.24E-16(R)	4.35E-01(UR) 4.24E-16(R)	3.72E-01(UR) 4.24E-16(R)	102859.19	114771.31	122199.66	126683.44
19	Newport-Inglewood	25.77	0.047	3.7E-02(UR) 2.06E-11 (R)	1.22E-03(UR) 7.25E-34(R)	1.39E-05(UR) 7.25E-34(R)	6.72E-06(UR) 7.25E-34(R)	377.91	421.67	448.96	465.44
20	Newport-Inglewood	39.62	0.029	3E-03(UR) 4.83E-17 (R)	3.23E-05(UR) 3.64E-39(R)	1.26E-07(UR) 3.64E-39(R)	5.23E-08(UR) 3.64E-39(R)	28.38	31.66	33.71	34.95
21	Newport-Inglewood	54.95	0.020	2.34E-04(UR) 4.83E-17 (R)	1.08E-06(UR) 1.62E-43(R)	1.83E-09(UR) 1.62E-43(R)	6.73E-10(UR) 1.62E-43(R)	2.23	2.48	2.65	2.74
22	Palos Verdes	25	0.048	4E-02 (UR) 2.73E-11 (R)	1.41E-03(UR) 1.21E-33(R)	1.68E-05(UR) 1.21E-33(R)	8.13E-06(UR) 1.21E-33(R)	665.41	742.47	790.53	819.53
23	San Andreas	70.17	0.015	2.31E-05(UR) 3.22E-19 (R)	5.36E-08(UR) 4.74E-47(R)	4.77E-11(UR) 4.74E-47(R)	1.6E-11(UR) 4.74E-47(R)	4.37	4.88	5.20	5.39
24	San Andreas	70.04	0.015	2.31E-05(UR) 3.22E-19 (R)	5.36E-08(UR) 4.74E-47(R)	4.77E-11(UR) 4.74E-47(R)	1.6E-11(UR) 4.74E-47(R)	4.37	4.88	5.20	5.39
25	San Jacinto	85.48	0.012	3.07E-06(UR) 5.27E-21 (R)	4.20E-09(UR) 6.86E-50(R)	2.25E-12(UR) 6.86E-50(R)	7.03E-13(UR) 6.86E-50(R)	0.29	0.33	0.35	0.36

26	Santa Susana	42.62	0.026	1E-03(UR) 3.51E-15 (R)	1.26E-05(UR) 2.03E-40(R)	3.85E-08(UR) 2.03E-40(R)	1.54E-08(UR) 2.03E-40(R)	141.45	157.83	168.05	174.22
27	San Fernando	34.05	0.034	7E-03(UR) 2.12E-13 (R)	1.18E-04(UR) 2.25E-37(R)	6.57E-07(UR) 2.25E-37(R)	2.86E-07(UR) 2.25E-37(R)	362.95	404.99	431.20	447.02
28	Sierra Madre	30.61	0.038	1.7E-02(UR) 1.07E-12 (R)	2.75E-04(UR) 3.78E-36(R)	1.96E-06(UR) 3.78E-36(R)	8.85E-07(UR) 3.78E-36(R)	1329.77	1483.77	1579.80	1637.77
29	Sierra Madre	45.27	0.025	1.3E-02 (UR) 1.88E-15 (R)	8.84E-06(UR) 7.1E-41(R)	2.48E-08(UR) 7.1E-41(R)	9.8E-09(UR) 7.1E-41(R)	109.01	121.64	129.51	134.26
30	Whittier	43.01	0.026	1E-03(UR)3.51E-15 (R)	1.3E-05(UR)2.03E-40(R)	3.85E-08(UR)2.03E-40(R)	1.54E-08(UR)2.03E-40(R)	21.22	23.68	25.21	26.13
31	Malibu Coast	28.01	0.064	1.2E-01 (UR) 1.10E-09 (R)	7.93E-03(UR) 1.09E-30(R)	1.77E-04(UR) 1.09E-30(R)	9.37E-05(UR) 1.09E-30(R)	203.29	226.83	241.51	250.37
32	Malibu Coast	30.08	0.060	9.7E-02(UR) 4.93E-10 (R)	5.52E-03(UR) 2.44E-31(R)	1.07E-04(UR) 2.44E-31(R)	5.57E-05(UR) 2.44E-31(R)	159.04	177.45	188.94	195.87
33	Malibu Coast	10.42	0.165	7.65E-01(UR) 2.17E-05 (R)	3.02E-01(UR) 5.76E-22(R)	4.66E-02(UR) 5.76E-22(R)	3.27E-02(UR) 5.76E-22(R)	2180.04	2432.52	2589.95	2684.99
34	Newport-Inglewood	8.053	0.205	8.76E-01(UR) 1.29E-04 (R)	4.67E-01(UR) 3.48E-20(R)	1.07E-01(UR) 3.48E-20(R)	7.96E-22(UR) 3.48E-20(R)	18257.72	20372.15	21690.70	22486.58

35	Newport-Inglewood	31.08	0.058	8.6E-02 (UR) 3.22E-10 (R)	4.54E-03(UR) 1.1E-31(R)	8.18E-05(UR) 1.1E-31(R)	4.21E-05(UR) 1.1E-31(R)	463.98	517.71	551.22	571.44
36	Newport-Inglewood	53.83	0.033	6E-03 (UR) 1.36E-13(R)	9.31E-05(UR) 1.04E-37(R)	4.86E-07(UR) 1.04E-37(R)	2.09E-07(UR) 1.04E-37(R)	30.63	34.18	36.39	37.73
37	San Andreas	67.93	0.026	1E-03 (UR) 3.51E-15 (R)	1.26E-05(UR) 2.03E-40(R)	3.85E-08(UR) 2.03E-40(R)	1.54E-08(UR) 2.03E-40(R)	113.16	126.27	134.44	139.37
38	San Andreas	69.22	0.025	1E-03 (UR) 1.88E-15(R)	8.84E-06(UR) 7.1E-41(R)	2.48E-08(UR) 7.1E-41(R)	9.8E-09(UR) 7.1E-41(R)	87.21	97.31	103.61	107.41
39	San Jacinto	88.25	0.020	2.34E-04(UR) 4.84E-17 (R)	1.08E-06(UR) 1.62E-43(R)	1.83E-09(UR) 1.62E-43(R)	6.73E-10(UR) 1.62E-43(R)	11.13	12.42	13.23	13.71
40	Santa Susana	33.53	0.053	6.1E-02 (UR) 1.01E-10(R)	2.6E-03(UR) 1.31E-32(R)	3.91E-05(UR) 1.31E-32(R)	1.96E-05(UR) 1.31E-32(R)	705.36	787.05	837.99	868.73
41	Whittier	49.55	0.036	1E-02(UR) 4.91E-13 (R)	1.83E-04(UR) 9.64E-37(R)	1.16E-06(UR) 9.64E-37(R)	5.14E-07(UR) 9.64E-37(R)	99.59	111.13	118.32	122.66
42	Malibu Coast	10.82	0.202	8.7E-01(UR) 1.14E-04 (R)	4.55E-01(UR) 2.65E-20(R)	1.01E-01(UR) 2.65E-20(R)	7.54E-02(UR) 2.65E-20(R)	1765.26	1969.69	2097.18	2174.13
43	Malibu Coast	24.11	0.104	4.2E-01(UR) 2.70E-07 (R)	7.47E-02(UR) 5.04E-26(R)	4.64E-03(UR) 5.04E-26(R)	2.85E-03(UR) 5.04E-26(R)	324.05	361.58	384.99	399.11

44	San Jacinto	87.69	0.033	6E-03(UR) 1.36E-13 (R)	9.31E-05(UR) 1.04E-37(R)	4.86E-07(UR) 1.04E-37(R)	2.09E-07(UR) 1.04E-37(R)	91.90	102.54	109.18	113.19
45	San Andreas	66.26	0.042	2.2E-02(UR)4.40E-12 (R)	5.67E-04(UR)4.59E-35(R)	5.05E-06(UR)4.59E-35(R)	2.35E-06(UR)4.59E-35(R)	664.15	741.06	789.03	817.98
46	San Andreas	74.02	0.038	1.3E-02 (UR) 1.07E-12 (R)	2.75E-04(UR) 3.78E-36(R)	1.96E-06(UR) 3.78E-36(R)	8.85E-07(UR) 3.78E-36(R)	398.93	445.13	473.94	491.33
47	Whittier	45.35	0.059	9.1E-02 (UR) 3.99E-10(R)	5.01E-03(UR) 1.65E-31(R)	9.38E-05(UR) 1.65E-31(R)	4.85E-05(UR) 1.65E-31(R)	496.42	553.91	589.76	611.40
TOTAL ANNUAL BENEFIT								237510.45	265016.54	282169.22	292522.63
BENEFIT-COST RATIO								1.42	1.59	1.69	1.75